

Local Loss Optimization in the Infinite Width: Stable Parameterization of Predictive Coding Networks and Target Propagation

Satoki Ishikawa

Department of Computer Science
Institute of Science Tokyo, Japan
ishikawa@rio.scrs.iir.isct.ac.jp

Rio Yokota

Institute of Integrated Research
Institute of Science Tokyo, Japan
rioyokota@rio.scrs.iir.isct.ac.jp

Ryo Karakida

Artificial Intelligence Research Center
AIST, Japan
karakida.ryo@aist.go.jp

Abstract

Local learning, which trains a network through layer-wise local targets and losses, has been studied as an alternative to backpropagation (BP) in neural computation. However, its algorithms often become more complex or require additional hyperparameters because of the locality, making it challenging to identify desirable settings in which the algorithm progresses in a stable manner. To provide theoretical and quantitative insights, we introduce the maximal update parameterization (μ P) in the infinite-width limit for two representative designs of local targets: predictive coding (PC) and target propagation (TP). We verified that μ P enables hyperparameter transfer across models of different widths. Furthermore, our analysis revealed unique and intriguing properties of μ P that are not present in conventional BP. By analyzing deep linear networks, we found that PC's gradients interpolate between first-order and Gauss-Newton-like gradients, depending on the parameterization. We demonstrate that, in specific standard settings, PC in the infinite-width limit behaves more similarly to the first-order gradient. For TP, even with the standard scaling of the last layer, which differs from classical μ P, its local loss optimization favors the feature learning regime over the kernel regime.

1 Introduction

Deep learning has achieved remarkable performance by building upon the backpropagation (BP) algorithm and developing architectures specialized for it [Rumelhart et al., 1986, LeCun et al., 1998, 2015]. BP, however, is not always a suitable method for more general objectives, such as biologically plausible computation [Lillicrap et al., 2020, Bredenberg et al., 2024] or efficient distributed computation [Amid et al., 2022]. A representative alternative is local loss optimization, a type of credit assignment problem, in which loss functions are defined layer-wise, and targets are set locally. The basic formulation involves performing regression on target signals at each layer to reduce the global error across the entire network: Predictive Coding networks, usually referred to as PC, generate their targets through the internal dynamics of inference [Whittington and Bogacz, 2017, Song et al., 2020, Salvatori et al., 2023], while Target Propagation (TP) generates them using feedback networks [Bengio, 2014, Lee et al., 2015, Ernoult et al., 2022].

In many cases, the use of local losses requires additional hyperparameters (HPs) and their careful tuning, making the algorithm configuration significantly more complicated compared to that of BP. For example, PC requires not only the usual HPs, such as learning rate and initialization of weight parameters, but also those for the inference phase, such as the initialization of the state and the number of inference sequences. These HPs are primary considerations and have been reported as

critical for ensuring stable training behavior [Pinchetti et al., 2024, Alonso et al., 2024, Rosenbaum, 2022]. A few analyses have succeeded in providing theoretical intuition for such local learning algorithms by introducing specific conditions or additional corrections that bridge them to classical optimization formulations [Song et al., 2020, Alonso et al., 2022, Meulemans et al., 2020]. However, such conditions are not always met in practice and may not be commonly shared across the entire family of methods. To develop local learning that is more easily manageable across a broader range of settings, it is promising to establish a theoretical foundation that enables the analysis of natural learning dynamics under fewer constraints.

For standard BP, deep learning theory offers insights into the universal properties of learning [Bahri et al., 2020, Bartlett et al., 2021]. A key research focus in this area is understanding learning in the infinite-width limit, including studies on neural tangent kernel (NTK) and feature learning regimes [Jacot et al., 2018, Chizat et al., 2019, Mei et al., 2018, Bordenon and Pehlevan, 2022b]. In particular, Yang and Hu [2021] provided a unified perspective on the parameterizations that realize these learning regimes and proposed maximal update parameterization (μ P) as a unique scaling of HPs, such as random initialization and learning rates, that achieves feature learning in the infinite-width limit. Building on this developing theoretical foundation, we expect to gain universal insight into local learning, which has not yet been systematically analyzed.

In this work, we derive the μ P for PC and TP and investigate hyperparameter transfer (the so-called μ Transfer) across different widths. Our contributions are summarized as follows:

- While it is known that PC inference trivially reduces to gradient computation of BP under the fixed prediction assumption (FPA), a technical and heuristic condition, there is generally no guarantee that PC will reduce to BP, making it highly non-trivial to identify its μ P. We first consider PC with a single sequential inference and reveal the μ P even without FPA (Theorem 4.1). We also empirically verify the μ Transfer of learning rates, showing that the optimal learning rate does not depend on the order of width.
- Second, for a more general context involving multiple inference sequences, we consider the convergence of the inference phase. We find that, for deep linear networks, we can explicitly obtain the local targets and losses at the fixed point of the inference, which depend on inference step sizes (Theorem 4.2). Interestingly, it takes a similar form to the Gauss-Newton (GN) gradient, but it can reduce to the conventional first-order gradient descent (GD) depending on the parameterization and step sizes. We find that the eventual gradient is closer to GD for sufficiently wide neural networks under standard experimental settings with μ P. We also confirm that a larger inference step size, identified through this analysis, enhances μ Transfer of HPs.
- Finally, we derive μ P for both TP and its variant difference target propagation (DTP) assuming linear feedback networks (Theorem 5.1). We reveal a distinct property that differs from BP and PC; the feedback network of (D)TP changes the preferable scale of the last layer compared to the usual μ P and causes the absence of the kernel regime. In this sense, (D)TP favors feature learning more strongly than other learning methods.

Thus, this study provides a solid and qualitative foundation for the further development of local learning schemes in large-scale neural networks in the future.

2 Related Work

Local learning: Most research on local learning stems from the exploration of biologically plausible learning [Lillicrap et al., 2020], with PC and TP following this line. As deep learning has evolved, local learning has also begun to focus on large-scale networks, and some models have achieved performances close to those trained with BP [Ernoul et al., 2022, Ren et al., 2023]. Several algorithms are inherently structured to resemble the BP chain [Akrou et al., 2019] or to estimate first-order gradients [Scellier and Bengio, 2017]. In contrast, PC relies on an inference phase, and TP uses a feedback network, both of which are quite different from BP and seems to be fundamental designs for using local targets. However, their optimization properties are still not well understood. Alonso et al. [2022] proposed a modified PC as a proximal point algorithm (implicit SGD), though it requires additional corrections and adaptive rescaling [Alonso et al., 2024]. Innocenti et al. [2023] proposed an inference phase computed by a GN method, but it requires a quadratic approximation of the local loss around a special initialization. As discussed in the next section, bridging to such classical

optimization requires strong conditions that may deviate significantly from the original purpose and algorithm [Rosenbaum, 2022, Meulemans et al., 2020].

Infinite width and μP : While the NTK regime guarantees the existence of learning dynamics in the infinite-width limit and its global convergence, it reduces to just a kernel method [Jacot et al., 2018, Lee et al., 2019]. To realize feature learning in the infinite-width limit, Yang and Hu [2021] proposed μP , which is a non-trivial scaling of HPs with respect to the width. From a theoretical perspective, this serves as a parameterization that enables the dynamics of feature learning, such as those described by the mean-field regime [Mei et al., 2018] or the dynamical mean-field theory [Bordelon and Pehlevan, 2022b]. For more applications, μP or its extension has been validated across various architectures [Yang et al., 2021, Vyas et al., 2023, Everett et al., 2024]. It covers not only the naive first-order gradient but also entry-wise adaptive optimizers such as Adam [Yang and Littwin, 2023] and second-order optimization methods like K-FAC [Ishikawa and Karakida, 2024]. There has been little previous work on the infinite-width analysis of local learning. Bordelon and Pehlevan [2022a] formulated (direct) feedback alignment and (supervised) Hebbian learning using dynamical mean-field theory, which are rather close to BP.

3 Preliminaries

In this section, we provide an overview of local learning and μP in an L -layer fully connected neural network:

$$h_l = \phi(u_l), \quad u_l = W_l h_{l-1} \quad (l = 1, \dots, L), \quad (1)$$

where $W_l \in \mathbb{R}^{M_l \times M_{l-1}}$ are weight matrices, $h_l, u_l \in \mathbb{R}^{M_l \times N}$ are activations and N is the number of samples, independent of the order of width M . We set the width of the hidden layers to $M_l = M$ for $(l = 1, \dots, L-1)$ for simplicity. To keep the notation concise, for non-linear networks, we set $M_L = 1$; however, we can easily generalize to $M_L = \Theta(1)$. The activation function $\phi(\cdot)$ is usually assumed to be differentiable and polynomially bounded for some theoretical reasons within the μP framework [Yang and Hu, 2021].

3.1 Overview of Local Learning

3.1.1 Predictive Coding

Predictive Coding updates both the states and weights to minimize the following free-energy function [Whittington and Bogacz, 2017, Song et al., 2020, Salvatori et al., 2023]:

$$\mathcal{F}(v, W) = \gamma_L \mathcal{L}(y, W_L \phi(v_{L-1})) + \sum_{l=1}^{L-1} \gamma_l \frac{1}{2} \|v_l - W_l \phi(v_{l-1})\|^2. \quad (2)$$

To distinguish the internal state from the forward signal propagation u_l , we denote this state as v_l . Although this algorithm was originally derived from the variational Bayes formulation, it has been extended beyond the scope of the original framework, aiming instead to develop inference computations that work more effectively in practice. PC is composed of two phases: an inference phase, in which the per-layer states v_l are updated and a learning phase, in which weights W_l are updated. Its update rule for the inference phase is given by

$$v_{l,s+1} = v_{l,s} - \frac{\partial \mathcal{F}}{\partial v_l} = v_{l,s} - \gamma_l e_{l,s} + \gamma_{l+1} \phi'(v_{l,s}) \circ W_{l+1}^\top e_{l+1,s}, \quad (3)$$

where we define $e_{l,s} := v_{l,s} - W_l \phi(v_{l-1,s})$ and \circ denotes the Hadamard product. The update rule for the learning phase is given by

$$W_{l,t+1} = W_{l,t} - \eta_l \frac{\partial \mathcal{F}}{\partial W_l} = W_{l,t} + \eta_l \gamma_l e_{l,s} \phi(v_{l-1,s})^\top. \quad (4)$$

Note that the inference time index s and the parameter update index t are distinct with s resetting to 0 at each t . We usually omit the step size γ_l in Eq. (4) in implementation. Generally, weights are updated after multiple inference steps, while incremental version of PC (iPC), which updates the weights after just a single inference, has also been proposed [Salvatori et al., 2024]. The internal state can be updated simultaneously across all layers or computed sequentially in a specified order. In the first part of the next section, we focus on the Sequential Inference (SI) method, where $e_{l,s}$ is

computed sequentially by propagating from the output layer to the input layer. For more details on this difference, see Algorithm 1 in the Appendix.

Empirically, to improve the trainability, PC often relies on assumptions that are either rational or, at times, unrealistic. One such reasonable assumption is the initialization method for $v_{l,0}$, which is used to improve the convergence [Song et al., 2020, Alonso et al., 2022, Rosenbaum, 2022]:

Technique (i): Forward initialization (F-ini). At each training step t , $v_{l,0}$ is initialized such that $v_{l,0} = u_{l,t}$, which ensures $e_{l,0} = 0$.

Generally, the gradient computation of PC does not match that of BP. However, under F-ini and SI, it reduces to BP by adopting the following rather technical assumption [Millidge et al., 2022b, Rosenbaum, 2022]:

Technique (ii): Fixed prediction assumption (FPA). Replace $\phi(v_{l-1,s})$ with $\phi(v_{l-1,0})$ during the inference phase.

Under FPA, the inference is given by $e_{l,s+1} = (1 - \gamma_l)e_{l,s} + \gamma_{l+1}\phi'(v_{l,0}) \circ W_{l+1}^\top e_{l+1,s}$. By substituting F-ini, one can easily verify that this sequential inference computes $\nabla_{u_l} \mathcal{L}$.

3.1.2 Target Propagation

In target propagation (TP), $\hat{h}_L = h_L - \hat{\eta} \nabla_{h_L} \mathcal{L}$ is propagated through the feedback network, which generates local targets \hat{h}_l as follows:

$$\hat{h}_l = g_l(\hat{h}_{l+1}), \quad g_l(x) = \psi(Q_l x) \quad (l = 1, \dots, L-1), \quad (5)$$

where $Q_l \in \mathbb{R}^{M_{l-1} \times M_l}$ are weight matrices. We also analyze the Difference Target Propagation (DTP), a variant of TP, whose definition is provided in the appendix. The feedback network is trained to minimize the following reconstruction loss:

$$\mathcal{L}_{\text{rec}}(Q_l) = \|g_l(f_l(h_{l-1})) - h_{l-1}\|^2, \quad (6)$$

where $f_l(x) = \phi(W_l x)$. TP updates the weights W_l to minimize the following local loss $\|e_l\|^2 := \|\hat{h}_l - h_l\|^2$. The gradient of this local loss provides the update rule for the learning phase as $W_{l,t+1} = W_{l,t} - \eta_l \phi'(W_{l,t} h_{l-1}) \circ e_l h_{l-1}^\top$. For a so-called invertible network, TP computes the Gauss-Newton Target (GNT), i.e., $e_l^{\text{GNT}} = (\delta_l \delta_l^\top + \rho I)^{-1} \delta_l e_L$ where $\delta_l = \nabla_{u_l} u_L$ is the BP signal [Meulemans et al., 2020]¹. Note that the assumption of the invertible network is restrictive because the invertible network requires invertible activation functions, regular weight matrices, and the training tp converge to the solution of $g_l(\hat{h}_{l+1}) = f_{l+1}^{-1}(\hat{h}_{l+1}) = W_{l+1}^{-1} \phi^{-1}(\hat{h}_{l+1})$. For general networks, (D)TP does not necessarily lead to the GNT.

Remark on a connection between PC and TP. Some previous studies have argued that PC yields GNT-like solutions, and thus can be connected to TP [Alonso et al., 2022, Millidge et al., 2022a]. These works attempt to gain an intuitive insight from the fixed point equation for each layer:

$$h_l^* = (W_{l+1}^\top W_{l+1} + \gamma_{l+1}/\gamma_l I)^{-1} (W_{l+1}^\top h_{l+1}^* + \gamma_{l+1}/\gamma_l W_l h_{l-1}^*), \quad (7)$$

where h_l^* means $\phi(v_l^*)$. For $\gamma_{l+1}/\gamma_l \ll 1$, we approximate $h_l^* \approx W_{l+1}^\dagger h_{l+1}^*$. If we multiply this approximation across layers, the naive expectation is that $h_l^* \approx \prod_{i=l+1}^L W_i^\dagger e_L^*$, which corresponds to the GNT for linear networks. Thus, we can intuitively see that the PC may be linked to the GNT, although its exact connection requires careful limit operations across layers. Additionally, taking the limits $\gamma_{l+1}/\gamma_l \ll 1$ for all layers means the exponential decay of γ_l with depth, raising concerns regarding its practical relevance. For $\gamma_l = 1$, Innocenti et al. [2024] has recently derived an explicit formulation of the free energy at the fixed point using an unfolding calculation of a hierarchical Gaussian model. This fomulation shows that the obtained gradient differs from that of the exact GNT, supporting the idea that the connection to GNT would be weak.

3.2 μP and Learning Regimes

The abc-parameterization scales the parameters by width, as follows [Yang and Hu, 2021]:

$$W_l = w_l/M^{a_l}, \quad w_l \sim \mathcal{N}(0, \sigma'^2/M^{2b_l}), \quad \eta_l = \eta'_l/M^{c_l}. \quad (8)$$

¹The final gradient $d\mathcal{F}/dW_l$ is equivalent to the special case of K-FAC [Martens and Grosse, 2015] where the preconditioners are applied only to the backward signals.

Table 1: Parameterization (b_l, c_l) . PC with $\bar{\gamma}_L = 0$ reduces to SGD’s μP , while one with $\bar{\gamma}_L = -1$ reduces to GNT’s. TP has the distinctive property of $b_L = 1/2$.

Layer	SP	SGD	GNT	PC	TP
Input	$(0, 0)$	$(0, -1)$	$(0, 0)$	$(0, -\bar{\gamma}_L - 1)$	$(0, 0)$
Hidden	$(1/2, 0)$	$(1/2, 0)$	$(1/2, 1)$	$(1/2, -\bar{\gamma}_L)$	$(1/2, 1)$
Output	$(1/2, 0)$	$(1, 1)$	$(1, 1)$	$(1, 1)$	$(1/2, 1)$

μP and its conditions: Consider the temporal change of u_l by the parameter update:

$$\Delta u_{l,t} := u_{l,t} - u_{l,0} = \Theta(1/M^{r_l}), \quad (9)$$

where $\Theta(\cdot)$ denotes the order with respect to the width and $x = \Theta(M^a)$ means $\sqrt{\|x\|^2/M} = \Theta(M^a)$ for $x \in \mathbb{R}^M$. Yang and Hu [2021] characterized the condition where $r_l = 0$ for all layers as the feature learning regime and the condition where $r_{l < L} > 0$ and $r_L = 0$ as the kernel regime. The parametrization that induces the feature learning regime is called μP , while the NTK parametrization corresponds to the kernel regime with $r_{l < L} = 1/2$. The training dynamics are referred to as *stable* when they neither vanish nor explode as the network width increases; the parameterization that achieves this is called a stable parameterization. Yang and Hu [2021] demonstrated that the concrete evaluation of feature learning with $r_l = 0$ reduces to the following two conditions:

Condition 3.1 (W_l updated maximally). $\Delta W_{l,t} h_{l-1,t} = \Theta(1)$ where $\Delta W_{l,t} := W_{l,t} - W_{l,0}$.

Condition 3.2 (W_L initialized maximally). $W_{L,0} \Delta u_{L-1,t} = \Theta(1)$.

Note that the original derivation of the parametrization that satisfies the above conditions is based on the first (infinitesimal) one-step update of the parameters [Yang and Hu, 2021, Ishikawa and Karakida, 2024]. Our work also follows the same approach.

3.2.1 μP for Gauss-Newton Target

The following work has recently derived the μP scaling, including both first-order and second-order optimizations.

Proposition 3.3 (Ishikawa and Karakida [2024]). *Consider the first one-step update by the GNT: $W_{l,1} = W_{l,0} - \eta_l \phi'(W_{l,t} h_{l-1}) \circ (\delta_l \delta_l^\top + \rho I)^{-e_B} \delta_l \text{diag}(e_L) h_{l-1}^\top$. In the infinite-width limit, this update admits the μP for feature learning at*

$$\begin{cases} \theta_1 = e_B - 1, & \theta_{1 < l < L} = e_B, & \theta_L = 1 \\ b_1 = 0, & b_{1 < l < L} = 1/2, & b_L = 1, \end{cases} \quad (10)$$

where $\theta_l := 2a_l + c_l$. We obtain μP of SGD for $e_B = 0$, and that of GNT for $e_B = 1$.

More precisely, we can also allow $b_L \geq 1$ for the feature learning regime. However such initialization eventually reduces to the case of $b_L = 1$ in the next parameter update. Thus, we effectively summarize it as $b_L = 1$. The scaling of $b_L = 1$ implies that a smaller initialization is required compared to the standard parametrization (SP), which is PyTorch’s default, for sufficiently wide neural networks. It can also be immediately verified that we can set $a_l = 0$ due to shift invariance without loss of generality. In Table 1, we summarize the μP from previous work and our results obtained in the following sections.

4 Feature Learning of predictive coding

4.1 μP of PC with single-shot sequential inference

As noted in the preliminary section, PC involves such techniques as F-ini, SI, and FPA, which must be clearly distinguished when deriving the μP . It is well-established that when F-ini, SI, and FPA are all assumed, PC reduces to the gradient computation of BP, and the μP should match the one from standard BP. Figure 1 shows that when F-ini, FPA, and SI are applied, the μP of BP can be directly transferred to PC.

However, this may not hold for general PC and BP as there is no guarantee of their equivalence. To explore this, we first remove FPA. Although initialization (F-ini) and sampling (SI) are inherently

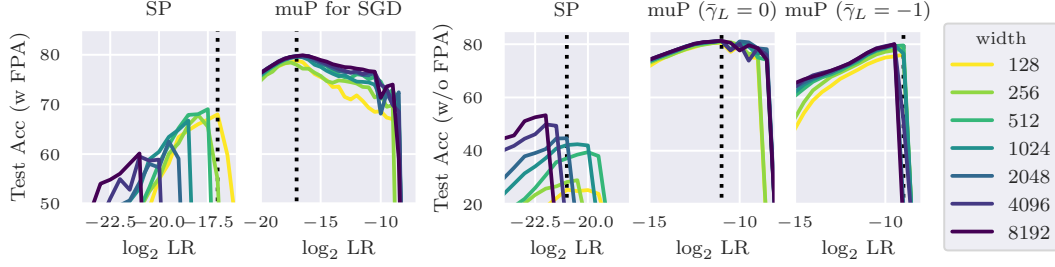


Figure 1: $\mu\mathbf{P}$ enables the transfer of learning rates across widths. (Left) PC reduces to SGD, when F-ini, FPA and SI are applied. In fact, using the $\mu\mathbf{P}$ of SGD, learning rates are successfully transferred across different widths. (Right) Even without FPA, our $\mu\mathbf{P}$ of PC also allows μ Transfer across widths. In this case, inference is performed only once and the difference in test accuracy between $\bar{\gamma}_L = 0$ and $\bar{\gamma}_L = 1$ is small. Both figures show results for training a 3-layer MLP on FashionMNIST.

arbitrary, the justification for FPA is unclear from both machine learning and biological perspectives. In PC without FPA, we find the $\mu\mathbf{P}$ as follows:

Theorem 4.1 ($\mu\mathbf{P}$ for PC (informal)). *Let the inference step sizes be $\gamma_{l<L} = \Theta(1)$ and $\gamma_L = \gamma'/M^{\bar{\gamma}_L}$ with a positive constant γ' . Consider the first one-step update of the learning parameters after a first single-shot SI with F-initialization. Then, PC admits the $\mu\mathbf{P}$ for feature learning at*

$$\begin{cases} \theta_1 = -\bar{\gamma}_L - 1, & \theta_{1<l<L} = -\bar{\gamma}_L \geq 0, & \theta_{l=L} = 1, \\ b_1 = 0, & b_{l<L} = 1/2, & b_L = 1. \end{cases} \quad (11)$$

Rough sketch of the derivation. Section A.2 of the Appendix presents a detailed and comprehensive derivation. It is based on the perturbation approach, which applies to general networks with nonlinear activation functions. This method is inspired by the previous work that derived the $\mu\mathbf{P}$ by evaluating Conditions 3.1 and 3.2 using the perturbations, such as $\partial_{\eta'}(\Delta W_{l,1}h_{l-1,1})|_{\eta'=0} = \Theta(1)$. This allows for a systematic and transparent derivation. In PC, we extend the perturbation argument to the inference step size and require

$$\partial_{\gamma'}\partial_{\eta'}(\Delta W_{l,1}h_{l-1,1})|_{\eta'=\gamma'=0} = \Theta(1), \quad (12)$$

which is an example of Condition 3.1 for the hidden layer. Under the assumption of F-ini ($e_{l,0} = 0$), by putting $\delta_l = \nabla_{u_l}\mathcal{L}$, we obtain $u_{l,1} - u_{l,0} = -\prod_{i=l+1}^L \gamma_i \delta_i$, and

$$e_{l,1} = (u_{l,0} - \prod_{i=l+1}^L \gamma_i \delta_i) - \phi(W_{l,0}(u_{l-1,0} - \prod_{i=l}^L \gamma_i \delta_{l-1})). \quad (13)$$

For the hidden layers, this leads to

$$\partial_{\gamma'}\partial_{\eta'}(\Delta W_{l,1}h_{l-1,1})|_{\eta'=\gamma'=0} = \frac{1}{M^{\theta_l+\bar{\gamma}_L}} (-\delta_l + \phi'(W_l u_{l-1,0}) \circ W_l \delta_{l-1}) h_{l-1,0}^\top h_{l-1,0}. \quad (14)$$

We can similarly evaluate the other layers. Eventually, the $\mu\mathbf{P}$'s conditions become

$$\theta_1 + \bar{\gamma}_L + (a_L + b_L) = 0, \quad \theta_l + \bar{\gamma}_L - 1 + (a_L + b_L) = 0, \quad (15)$$

$$\theta_L - 1 = 0, \quad a_L + b_L - 1 = 0. \quad (16)$$

The last condition comes from Condition 3.2. We can derive the NTK parameterization of PC in the same way.

As Figure 1 demonstrates, the obtained $\mu\mathbf{P}$ supports μ Transfer in PC without FPA. This means that the optimal hyperparameters tuned for smaller-width models can be effectively re-used in larger-width models. Additionally, consistent with previous work, we observed the empirical rule of “wider is better” in $\mu\mathbf{P}$ [Yang et al., 2021], where test accuracy improves as the network width increases.

Thus far, when considering the parameter gradients, it appears that $\bar{\gamma}_L$ as a free parameter can be absorbed into the learning rate, allowing the feature learning dynamics to remain stable. However, as the following analysis shows, γ_L modifies the preconditioning of the computed gradients, which may influence μ Transfer of both γ_L itself and the learning rate. The analysis also demonstrates the validity of setting $\gamma_{l<L} = \Theta(1)$.

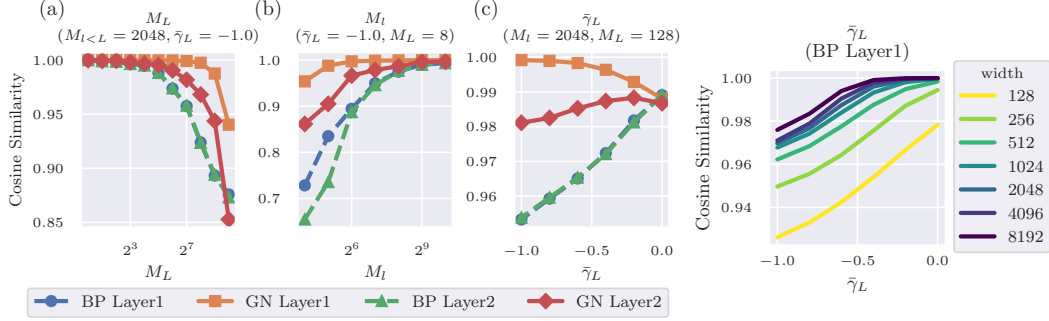


Figure 2: **(Left) Comparison of gradients with the analytical solution of a linear network.** (a) $\bar{\gamma}_L = 0$ yields gradients closer to BP gradient (which means GD in this experiment) compared to $\bar{\gamma}_L = -1$. (b) As M_L approaches 1, PC’s gradient converges to BP’s. (c) As M_L increases, the PC gradient approaches BP’s. **(Right) In a nonlinear MLP, PC’s gradient also approaches BP’s when $\bar{\gamma}_L = 0$.** This experiment was conducted using MLP with Tanh on the FashionMNIST dataset.

4.2 Analysis with Linear Network

In the previous section, we derived the μP under the assumption that inference is performed only once using F-ini and SI. However, in practice, the inference phase typically involves multiple update steps. To address this, we found that it is possible to explicitly derive the following general solutions (fixed points) of the inference phase for linear networks. See Section A.3 for the derivation.

Theorem 4.2. Suppose an L -layered linear network, where we put $e_l^* = v_l^* - W_l v_{l-1}^*$, with $*$ denoting the fixed point of the inference process(3). The following holds:

$$e_l^* = \frac{\gamma_L}{\gamma_l} W_{L:l+1}^\top (I + C_\gamma(W))^{-1} (W_{L:1}x - y), \quad C_\gamma(W) := \sum_{i=2}^L \frac{\gamma_L}{\gamma_{i-1}} W_{L:i} W_{L:i}^\top \quad (17)$$

$$v_l^* = W_{l:1}x + \left(\frac{\gamma_L}{\gamma_l} W_{L:l+1}^\top + \sum_{i=2}^{l-1} \frac{\gamma_L}{\gamma_{i-1}} W_{L:i} W_{L:i}^\top \right) (I + C_\gamma(W))^{-1} (y - f). \quad (18)$$

and $e_L^* = y - W_L v_{L-1}^* = (I + C_\gamma(W))^{-1} (W_{L:1}x - y)$ where $W_{L:i} = W_L W_{L-1} \dots W_i$.

From this general solution, we can also confirm the following property of the infinite width.

Corollary 4.3. Suppose the setting of Theorem 4.2, $\gamma_{l < L} = \Theta(1)$ and $a_L + b_L = 1$. In the infinite-width limit, the PC’s gradient reduces to GD for $\gamma_L = \Theta(1)$. For $\gamma_L = \Theta(M)$, the preconditioner part C_γ remains of order 1.

The exact solutions e_l^* provide much clearer insight into the gradient computation compared to Eq. (7), which was previously argued but not explicitly solved. First, it becomes evident that PC does not generally coincide with GNT. Consequently, PC is also generally different from TP. In fact, PC coincides with GNT only for the input layer in a shallow network (i.e., $L = 2$), where the update vector for PC corresponds to a GNT update with a damping term. Although PC does not entirely coincide with GNT, it is noteworthy that the scaling of c_l in μP for $\bar{\gamma}_L = -1$ matches that of GNT. In contrast, for $\bar{\gamma}_L = 0$, the PC’s gradient aligns with the (S)GD. Because the preconditioner part scales as $C_\gamma = O(1/M)$ in the infinite-width limit, we observe that $e_l^* = \delta_l$, which reduces to the GD. Naturally, μP matches that of GD in this case.

Second, the order of e_l^* in the analytical solution for the linear network matches the order of $e_{l,1}$ as derived in Theorem 4.1. Therefore, this theorem implies that in linear networks, the μP of PC would remain unchanged regardless of the presence of F-ini or the number of inference iterations. Moreover, as proved in Section A.3.2, the orders of e_l^* and $e_{l,1}$ align only when $\gamma_{l < L} = \Theta(1)$. In practical settings with multiple inferences, it is desirable for the μP to be consistent both when performing a single inference and after the inference has fully converged. Therefore, setting $\gamma_{l < L} = \Theta(1)$ is reasonable.

Additionally, we found that the dimension of the last layer plays a key role in determining the similarity between PC and BP. According to the solution for linear networks, when $M_L = 1$, the

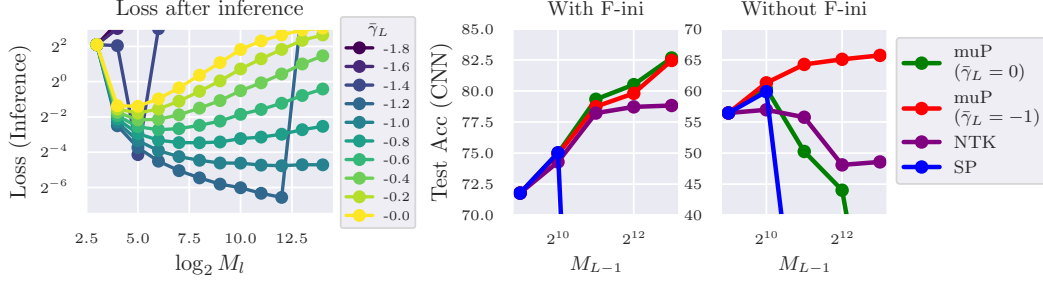


Figure 3: **(Left)** $\bar{\gamma}_L = -1$ steadily reduces the local loss as width increases. We observed the inference loss in a randomly initialized linear network for various $\bar{\gamma}_L$. For $\bar{\gamma}_L = -1$, the inference loss consistently decreases with increasing width. **(Right)** The "wider is better" trend holds for μP with $\bar{\gamma}_L = -1$. With F-ini, this trend holds for μP regardless of the $\bar{\gamma}_L$ value. However, without F-ini, the benefits of $\bar{\gamma}_L = -1$ become particularly prominent.

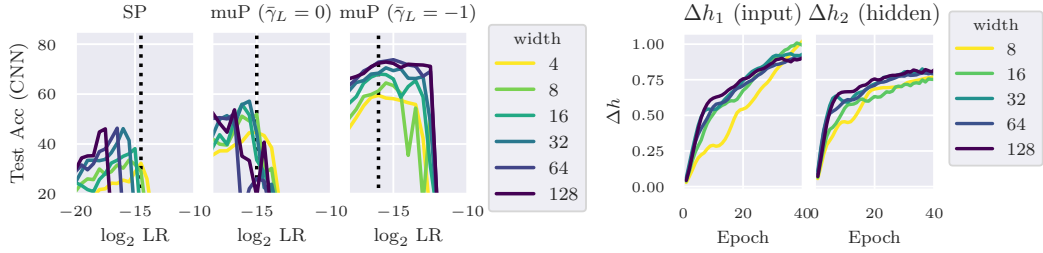


Figure 4: **(Left)** μP can transfer the learning rate across widths (without F-ini). We trained a 3-layer CNN on FashionMNIST with 100 inference iterations. Without F-ini, the stability of the inference becomes more crucial. As a result, unlike the single-shot SI with F-ini shown in Figure 1, the stability provided by $\bar{\gamma}_L = -1$ becomes critical. Note that additional experiments with different settings, including other architectures and loss functions, are presented in Section B.1.2 of the Appendix. **(Right)** Δh remains consistent across widths during training. We confirm that the condition $\Delta h = \Theta(1)$ required by μP holds throughout the training.

PC's gradient aligns with GD. Figure 2 shows numerical results confirming that for $M_L = 1$, the gradient direction always corresponds to GD, and for $M_l \gg M_L = \Theta(1)$, the gradient approaches GD as well. We observed that both GN and BP get much closer to each other for sufficiently large widths. In other words, even when we realize GNT by setting $\bar{\gamma}_L = -1$, it has a quite close direction. A detailed view of the cosine similarity at the large width is shown in Figure 2(c). This result seems reasonable because in the context of second-order optimization, it has also been reported that GNT tends to collapse into an identity matrix owing to damping [Benzing, 2022]. In summary, while PC's gradient switches between GD and GNT depending on the parameterization, it is important to highlight that GNT behaves similar to GD in the infinite-width limit.

As a minor extension, we can also analyze the nudge-type loss of PC defined by Eq. (S.86) [Alonso et al., 2022, Millidge et al., 2023, Pinchetti et al., 2024]. In this case, the damping term I in Eq. (17), is replaced by $(1 + \gamma/\beta)I$. Thus, the dependence on the parameterization remains essentially the same as that of the naive PC. Further discussion on nudge-type PC can be found in Appendix A.3.3.

4.3 Stability of inference phase

To ensure feature learning in SGD, the μP framework requires stable activations, i.e., $\Delta u_{l < L} = \Theta(1)$. It seems natural to apply this requirement to the inference phase of PC. That is, let us suppose $u_{l < L, s}$ varies by $\Theta(1)$ during the inference. Note that in Eq.(3) at $L-1$, the feedforward signal from the lower layer is $\gamma_{L-1} e_{L-1, s} = \Theta(1)$, and the error feedback from the last layer is $\gamma_L \phi'(u_{L-1, s}) \circ W_L^\top e_{L, s} = \Theta(1/M^{\bar{\gamma}_L + b_L - 1})$. Both terms should be of order $\Theta(1)$ for the inference to successfully merge both feedforward and feedback signals. When $b_L = 1$, this condition requires $\gamma_L = \Theta(M)$, and we can expect the local loss in the last layer e_L to decrease most prominently during the inference. Additionally for $\gamma_{l < L} = \Theta(1)$, the inference remains stable for layers $l < L-1$. Empirical results in Figure 3 (left) confirm that when $\bar{\gamma}_L = -1$, the inference loss decreases consistently as the width

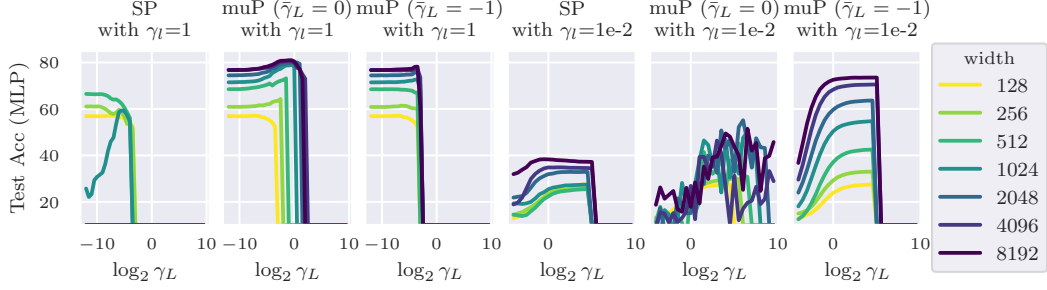


Figure 5: **μP with $\bar{\gamma}_L = -1$ performs consistently well, regardless of γ_L .** When γ_L is small ($\gamma_L = 0.01$), μP with $\bar{\gamma}_L = 0$ performs poorly, while μP with $\bar{\gamma}_L = -1$ shows significantly better performance. This difference is likely due to slower inference convergence in μP with $\bar{\gamma}_L = 0$. For larger values of γ_L ($\gamma_L = 1$), both μP configurations exhibit high accuracy. However, for μP with $\bar{\gamma}_L = 0$, γ_L does not transfer effectively across widths, whereas μP with $\bar{\gamma}_L = -1$ demonstrates the successful transfer of γ_L across widths.

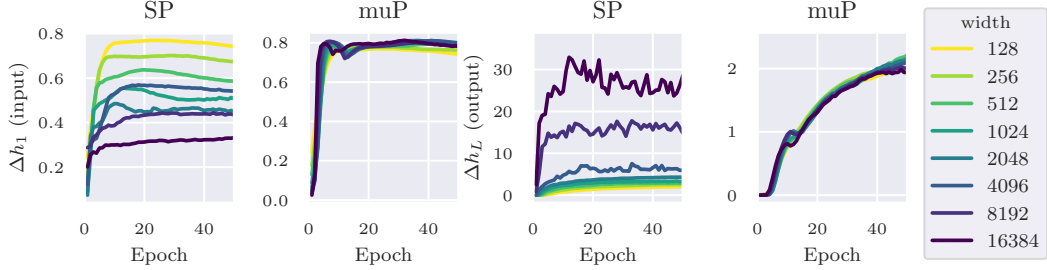


Figure 6: **In Target Prop, using μP ensures that Δh_l remains consistent across widths.** This figure shows the RMS norm of Δh_l during training. For SP, Δh_l in the input layer diminishes as the width increases, while Δh_l in the output layer diverges with increasing width. Consequently, the training dynamics become unstable. In contrast, with μP , Δh_l remains consistent across different widths in both the input and output layers.

increase, verifying that the “wider is better” hypothesis holds even in inference. This facilitates the hyperparameter transfer of γ_L for the inference dynamics.

We also observe the benefits of using $\bar{\gamma}_L = -1$ for the parameter updates. Without F-ini, the convergence of inference usually deteriorates for SP, making inference stability specially critical in this scenario. As shown in Figure 3 (right), the “wider is better” trend holds with F-ini regardless of $\bar{\gamma}_L$. However, without F-ini, this trend holds only when $\bar{\gamma}_L = -1$. Figure 4 demonstrates that the μ Transfer of the learning rate holds for $\bar{\gamma}_L = -1$. Additionally, Figure 5 indicates that $\bar{\gamma}_L = -1$ is also preferable from the perspective of μ Transfer of γ_L .

5 Feature Learning of target propagation

5.1 μP of TP

As overviewed in Section 3.1.2, TP reduces to GNT in the highly restrictive case of invertible networks. However, TP is not equivalent to GNT or BP in general cases [Meulemans et al., 2020, Ernoul et al., 2022]. While TP involves two networks trained using different manners, and one may feel it challenging to obtain a stable parameterization for learning, we demonstrate that, under the assumption that the feedback network uses a linear activation function ψ , we can systematically derive μP for both TP and DTP.

Theorem 5.1 (μP for TP and DTP (informal)). *Consider a linear feedback network. The forward network is allowed to have nonlinear activation functions. After the first training phase of Q_1 , take*

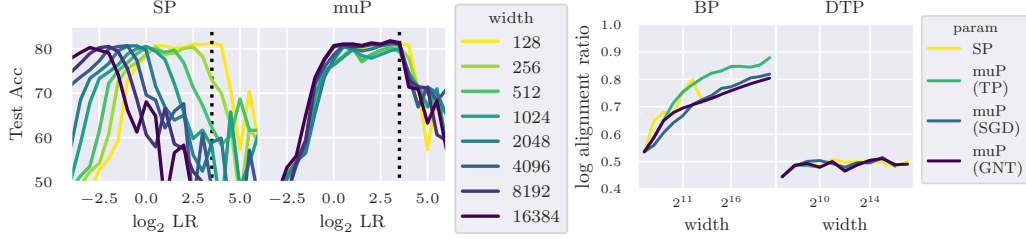


Figure 7: **(Left)** μP can transfer the learning rate across widths in TP. We trained a 3-layer MLP on FashionMNIST. **(Right)** TP does not have kernel regime. We measured $\omega_L = \log_M(\|W_{L,0}\Delta h_{L-1,T}\|_{\text{RMS}}/\|W_{L,0}\|_{\text{RMS}}\|\Delta h_{L-1,T}\|_{\text{RMS}})$ across different parametrizations following Everett et al. [2024]. In the infinite-width limit, ω_L converges to α . Therefore, in TP, where ω_L remains fixed at $1/2$ even as the width increases, the kernel regime disappears.

the first one-step update of W . Then, we obtain the μP as follows:

$$\begin{cases} c_1 = 0, & c_{1 < l < L} = 1, & c_L = 1, \\ b_1 = 0, & b_{1 < l < L} = 1/2, & b_L = 1/2. \end{cases} \quad (19)$$

The derivation is presented in Section A.4.1. Note that the linear feedback network has trained weights in a pseudo-inverse form, that is, $Q_l^* = h_{l-1}(h_l^\top h_l + \mu I)^{-1} h_l^\top$. Stable parametrization can also be discussed for the training of the feedback network. For further details, see Section A.5.

Figure 6 tracks Δh_l during training. In μP , Δh_l remains consistent across different widths, whereas in SP, Δh_l either diverges or diminishes as the width changes. As demonstrated in Figure 7, using the μP for TP results in the $\mu\text{Transfer}$ appropriately across widths.

5.2 Disappearance of the Kernel Regime

It is notable that μP in the previous work of the gradient methods requires $b_L = 1$; in TP, μP requires $b_L = 1/2$. For the usual gradient methods, a stable parametrization with $b_L = 1/2$ leads to the kernel regime. This raises the question: does a kernel regime exist in TP? Interestingly, in TP, the kernel regime disappears (see Corollary A.8 for the details).

Rough sketch of derivation. Condition 3.2 must hold to achieve stable learning in the hidden layers. Note that this condition is required in both the feature learning and kernel regimes. By expressing $\Delta h_{L-1} = \Theta(1/M^r)$, we obtain

$$a_L + b_L + r - \alpha = 0. \quad (20)$$

It is known that when the inner product $W_L \Delta h_{L-1}$ follows the Law of Large Numbers (LLN), $\alpha = 1$, and when it follows the Central Limit Theorem (CLT), $\alpha = 1/2$ [Everett et al., 2024]. Additionally, to prevent the output of the last layer from exploding, it is necessary that $h_L = O(1)$, that is, $a_L + b_L \geq 1/2$. Consequently, $r \leq \alpha - 1/2$. In BP, the dependence between W_L and Δh_{L-1} results in $\alpha = 1$ by the LLN. We have $r \leq 1/2$, allowing for the kernel regime. In contrast, in TP, updating the feedforward network weights does not induce a dependence between W_L and Δh_{L-1} , leading to $\alpha = 1/2$. This is because the gradient propagated from the last layer is computed based on the feedback weight $Q_L^* = h_{L-1}(h_L^\top h_L + \mu I)^{-1} h_L^\top$. This corresponds to a regression of the last layer by using the downstream layer as the basis. Consequently, $r \leq 0$ and the kernel regime cannot be achieved in TP.

Note that $\alpha = 1/2$ in TP is also empirically confirmed in Figure 7. TP seems to be the first example in the infinite-width limit where $b_L = 1/2$ induces feature learning.

6 Conclusion

In this work, we revealed μP for local loss optimization that can effectively scale toward the infinite width in a stable manner, supported by our analysis of linear networks. Our study covers two of the most fundamental settings: the local targets computed during the inference phase (i.e., PC) and the feedback network (i.e., TP). Although neither method generally reduces to BP or GNT, making gradient computation non-trivial, we identified the μP and highlighted its intriguing properties, such

as the gradient switching depending on the parameterization and the disappearance of the kernel regime. Additionally, we empirically confirmed that the derived μP facilitates hyperparameter transfer across widths.

Limitation and future direction. The derivation of μP assumes a one-step gradient and linear networks, although this prerequisite is not unique to our work [Yang, 2020, Yang et al., 2024]. Ensuring the existence of feature learning dynamics for more general steps in the infinite width limit would require the development of a tensor program. However, handling the dependencies between variables that differ from standard BP, such as those arising from the inference phase and feedback pass, is non-trivial and presents an interesting direction for future research. Additionally, it would also be valuable to explore the learning dynamics of local learning and its convergence properties by extending the infinite width theory or further analyzing of linear networks. We believe that understanding the universal behavior of large-scale limits will provide a foundation for the development of more effective algorithms.

References

- Mohamed Akrouf, Collin Wilson, Peter Humphreys, Timothy Lillicrap, and Douglas B Tweed. Deep learning without weight transport. In *Advances in Neural Information Processing Systems*, 2019.
- Nicholas Alonso, Jeffrey Krichmar, and Emre Neftci. Understanding and improving optimization in predictive coding networks. In *AAAI Conference on Artificial Intelligence*, volume 38, pages 10812–10820, 2024.
- Nick Alonso, Beren Millidge, Jeffrey Krichmar, and Emre O Neftci. A theoretical framework for inference learning. *Advances in Neural Information Processing Systems*, 35, 2022.
- Ehsan Amid, Rohan Anil, and Manfred Warmuth. Locoprop: Enhancing backprop via local loss optimization. In *International Conference on Artificial Intelligence and Statistics*, pages 9626–9642. PMLR, 2022.
- Yasaman Bahri, Jonathan Kadmon, Jeffrey Pennington, Sam S Schoenholz, Jascha Sohl-Dickstein, and Surya Ganguli. Statistical mechanics of deep learning. *Annual Review of Condensed Matter Physics*, 11(1):501–528, 2020.
- Peter L Bartlett, Andrea Montanari, and Alexander Rakhlin. Deep learning: a statistical viewpoint. *Acta Numerica*, 30:87–201, 2021.
- Yoshua Bengio. How auto-encoders could provide credit assignment in deep networks via target propagation. *arXiv preprint arXiv:1407.7906*, 2014.
- Frederik Benzing. Gradient descent on neurons and its link to approximate second-order optimization. In *International Conference on Machine Learning*, pages 1817–1853. PMLR, 2022.
- Blake Bordelon and Cengiz Pehlevan. The influence of learning rule on representation dynamics in wide neural networks. In *International Conference on Learning Representations*, 2022a.
- Blake Bordelon and Cengiz Pehlevan. Self-consistent dynamical field theory of kernel evolution in wide neural networks. *Advances in Neural Information Processing Systems*, 2022b.
- Colin Bredenberg, Ezekiel Williams, Cristina Savin, Blake Richards, and Guillaume Lajoie. Formalizing locality for normative synaptic plasticity models. In *Advances in Neural Information Processing Systems*, 2024.
- Lenaic Chizat, Edouard Oyallon, and Francis Bach. On lazy training in differentiable programming. In *Advances in Neural Information Processing Systems*, 2019.
- Maxence M Ernoult, Fabrice Normandin, Abhinav Moudgil, Sean Spinney, Eugene Belilovsky, Irina Rish, Blake Richards, and Yoshua Bengio. Towards scaling difference target propagation by learning backprop targets. In *International Conference on Machine Learning*, pages 5968–5987. PMLR, 2022.

- Katie E Everett, Lechao Xiao, Mitchell Wortsman, Alexander A Alemi, Roman Novak, Peter J Liu, Izzeddin Gur, Jascha Sohl-Dickstein, Leslie Pack Kaelbling, Jaehoon Lee, and Jeffrey Pennington. Scaling exponents across parameterizations and optimizers. In *International Conference on Machine Learning*, 2024.
- Mario Geiger, Leonardo Petrini, and Matthieu Wyart. Perspective: A phase diagram for deep learning unifying jamming, feature learning and lazy training. *arXiv:2012.15110*, 2020.
- Francesco Innocenti, Ryan Singh, and Christopher Buckley. Understanding predictive coding as a second-order trust-region method. In *ICML Workshop on Localized Learning*, 2023.
- Francesco Innocenti, El Mehdi Achour, Ryan Singh, and Christopher L Buckley. Only strict saddles in the energy landscape of predictive coding networks? *To appear in Advances in Neural Information Processing Systems*, 2024.
- Satoki Ishikawa and Ryo Karakida. On the parameterization of second-order optimization effective towards the infinite width. In *International Conference on Learning Representations*, 2024.
- Arthur Jacot, Franck Gabriel, and Clément Hongler. Neural tangent kernel: Convergence and generalization in neural networks. In *Advances in Neural Information Processing Systems*, 2018.
- Ido Kanter and Haim Sompolinsky. Associative recall of memory without errors. *Physical Review A*, 35(1):380, 1987.
- Ryo Karakida and Kazuki Osawa. Understanding approximate fisher information for fast convergence of natural gradient descent in wide neural networks. *Advances in Neural Information Processing Systems*, 33:10891–10901, 2020.
- Yann LeCun, Léon Bottou, Genevieve B Orr, and Klaus-Robert Müller. Efficient backprop. In *Neural Networks: Tricks of the Trade*, pages 9–50. Springer, 1998.
- Yann LeCun, Yoshua Bengio, and Geoffrey Hinton. Deep learning. *Nature*, 521(7553):436–444, 2015.
- Dong-Hyun Lee, Saizheng Zhang, Asja Fischer, and Yoshua Bengio. Difference target propagation. In *Machine Learning and Knowledge Discovery in Databases*, pages 498–515. Springer, 2015.
- Jaehoon Lee, Lechao Xiao, Samuel Schoenholz, Yasaman Bahri, Roman Novak, Jascha Sohl-Dickstein, and Jeffrey Pennington. Wide neural networks of any depth evolve as linear models under gradient descent. In *Advances in Neural Information Processing Systems*, 2019.
- Timothy P Lillicrap, Adam Santoro, Luke Marris, Colin J Akerman, and Geoffrey Hinton. Backpropagation and the brain. *Nature Reviews Neuroscience*, 21(6):335–346, 2020.
- James Martens and Roger Grosse. Optimizing neural networks with Kronecker-factored approximate curvature. In *International Conference on Machine Learning*, pages 2408–2417. PMLR, 2015.
- Song Mei, Andrea Montanari, and Phan-Minh Nguyen. A mean field view of the landscape of two-layer neural networks. *Proceedings of the National Academy of Sciences*, **115**:E7665–E7671, 2018.
- Alexander Meulemans, Francesco Carzaniga, Johan Suykens, João Sacramento, and Benjamin F Grewe. A theoretical framework for target propagation. In *Advances in Neural Information Processing Systems*, 2020.
- Beren Millidge, Yuhang Song, Tommaso Salvatori, Thomas Lukasiewicz, and Rafal Bogacz. A theoretical framework for inference and learning in predictive coding networks. *arXiv:2207.12316*, 2022a.
- Beren Millidge, Alexander Tschantz, and Christopher L Buckley. Predictive coding approximates backprop along arbitrary computation graphs. *Neural Computation*, 2022b.

- Beren Millidge, Yuhang Song, Tommaso Salvatori, Thomas Lukasiewicz, and Rafal Bogacz. Backpropagation at the infinitesimal inference limit of energy-based models: Unifying predictive coding, equilibrium propagation, and contrastive hebbian learning. In *International Conference on Learning Representations*, 2023.
- Luca Pinchetti, Chang Qi, Oleh Lokshyn, Gaspard Olivers, Cornelius Emde, Mufeng Tang, Amine M’Charrak, Simon Frieder, Bayar Menzat, Rafal Bogacz, et al. Benchmarking predictive coding networks—made simple. *arXiv:2407.01163*, 2024.
- Mengye Ren, Simon Kornblith, Renjie Liao, and Geoffrey Hinton. Scaling forward gradient with local losses. In *International Conference on Learning Representations*, 2023.
- Robert Rosenbaum. On the relationship between predictive coding and backpropagation. *Plos One*, 17(3):e0266102, 2022.
- David E Rumelhart, Geoffrey E Hinton, and Ronald J Williams. Learning representations by back-propagating errors. *Nature*, 323(6088):533–536, 1986.
- Tommaso Salvatori, Ankur Mali, Christopher L Buckley, Thomas Lukasiewicz, Rajesh PN Rao, Karl Friston, and Alexander Ororbia. Brain-inspired computational intelligence via predictive coding. *arXiv preprint arXiv:2308.07870*, 2023.
- Tommaso Salvatori, Yuhang Song, Yordan Yordanov, Beren Millidge, Lei Sha, Cornelius Emde, Zhenghua Xu, Rafal Bogacz, and Thomas Lukasiewicz. A stable, fast, and fully automatic learning algorithm for predictive coding networks. In *International Conference on Learning Representations*, 2024.
- Benjamin Scellier and Yoshua Bengio. Equilibrium propagation: Bridging the gap between energy-based models and backpropagation. *Frontiers in Computational Neuroscience*, 11:24, 2017.
- Yuhang Song, Thomas Lukasiewicz, Zhenghua Xu, and Rafal Bogacz. Can the brain do backpropagation?—exact implementation of backpropagation in predictive coding networks. In *Advances in Neural Information Processing Systems*, 2020.
- Nikhil Vyas, Alexander Atanasov, Blake Bordelon, Depen Morwani, Sabarish Sainathan, and Cengiz Pehlevan. Feature-learning networks are consistent across widths at realistic scales. In *Advances in Neural Information Processing Systems*, 2023.
- James CR Whittington and Rafal Bogacz. An approximation of the error backpropagation algorithm in a predictive coding network with local Hebbian synaptic plasticity. *Neural Computation*, 29(5): 1229–1262, 2017.
- Greg Yang. Tensor programs II: Neural tangent kernel for any architecture. *arXiv:2006.14548*, 2020.
- Greg Yang and Edward J. Hu. Feature learning in infinite-width neural networks. In *International Conference on Machine Learning*, volume 139, pages 11727–11737. PMLR, 2021.
- Greg Yang and Etai Littwin. Tensor programs IVb: Adaptive optimization in the infinite-width limit. *International Conference on Learning Representations*, 2023.
- Greg Yang, Edward J Hu, Igor Babuschkin, Szymon Sidor, Xiaodong Liu, David Farhi, Nick Ryder, Jakub Pachocki, Weizhu Chen, and Jianfeng Gao. Tuning large neural networks via zero-shot hyperparameter transfer. In *Advances in Neural Information Processing Systems*, 2021.
- Greg Yang, Dingli Yu, Chen Zhu, and Soufiane Hayou. Feature learning in infinite-depth neural networks. In *International Conference on Learning Representations*, 2024.

Appendices

A Derivation of Stable Parameterization

A.1 Conditions

We follow the derivation based on the infinitesimal one-step update from random initialization [Yang and Hu, 2021, Ishikawa and Karakida, 2024], which involves taking the limit of a sufficiently small coefficient of the learning rate η' . This formulation clarifies the proof and enables the systematic derivation of μP across various problems. In the infinitesimal formulation, Conditions 3.1 and 3.2 are expressed as follows:

Condition A.1 (W_l updated maximally).

$$\partial_{\eta'} \Delta W_l h_{l-1,1} \big|_{\eta'=0} = \Theta(1) \quad (\text{S.1})$$

where $\Delta W_l := W_{l,1} - W_{l,0}$.

Condition A.2 (W_L initialized maximally).

$$\partial_{\eta'} W_{L,0} \Delta u_{L-1,1} \big|_{\eta'=0} = \Theta(1). \quad (\text{S.2})$$

In addition, the stability of learning is defined as follows (see Definition H.4 in Yang and Hu [2021] for more detail):

Definition A.3 (Stability of learning).

$$\Delta h_{l,t} = O(1). \quad (\text{S.3})$$

As described in the previous work [Yang and Hu, 2021, Ishikawa and Karakida, 2024], Condition 3.1 (or A.1) is required from the expansion of Eq. (9) by the parameter update, yielding

$$\partial_{\eta'} \Delta W_l h_{l-1,1} \big|_{\eta'=0} = \Theta(1/M^{r_l}), \quad (\text{S.4})$$

for abc-parameterization. The stability requires

$$r_l \geq 0 \quad (\text{S.5})$$

and, in particular, feature learning is characterized by $r_l = 0$. Condition 3.2 (or A.2) is required to eliminate a uninteresting case in which the hidden layer provides no contribution to the network output. Both NTK and feature learning regimes are characterized by this condition.

As is common in the μP theory, we also assume that the firing activities are of order 1 at random initialization:

Assumption A.4. $u_{l,0}, h_{l,0} = \Theta(1) \quad (l < L), \quad f_0 = u_{L,0} = O(1)$.

As shown in Theorem H.6 of Yang and Hu [2021], this assumption immediately leads to

$$a_1 + b_1 = 0, \quad a_{1 < l < L} + b_{1 < l < L} = 1/2, \quad a_L + b_L \geq 1/2. \quad (\text{S.6})$$

A.2 Predictive Coding with single-shot SI

Theorem A.5 (Stable parameterization for PC). *Set inference step sizes $\gamma_{l < L} = \Theta(1)$ and $\gamma_L = \gamma'/M^{\tilde{\gamma}_L}$ with a positive constant γ' . Suppose F -initialization and single-shot sequential inference, and consider one-step update of parameters after the inference. For infinitesimal step sizes γ'_L and η' , PC admits the μP for feature learning at*

$$\begin{cases} c_1 = -\tilde{\gamma}_L - 1, & c_{1 < l < L} = -\tilde{\gamma}_L, & c_{l=L} = 1, \\ b_1 = 0, & b_{l > L} = 1/2, & b_l = 1. \end{cases} \quad (\text{S.7})$$

Additionally, it admits the NTK parametrization at

$$\begin{cases} c_1 = -\tilde{\gamma}_L, & c_{1 < l < L} = 1 - \tilde{\gamma}_L, & c_L = 1 \\ b_1 = 0, & b_{l < L} = 1/2. \end{cases} \quad (\text{S.8})$$

Proof. Assuming F-ini, considering the single-shot SI for v_l , we have

$$v_{l,1} = v_{l,0} + \gamma_{l+1} \phi'(v_{l,0}) \circ W_{l+1}^\top e_{l+1,1} \quad (\text{S.9})$$

$$= v_{l,0} + \gamma_{l+1} \phi'(v_{l,0}) \circ W_{l+1}^\top (v_{l+1,1} - W_{l+1} h_{l,0}) \quad (\text{S.10})$$

$$= v_{l,0} + \gamma_{l+1} \phi'(v_{l,0}) \circ W_{l+1}^\top (v_{l+1,1} - v_{l+1,0}), \quad (\text{S.11})$$

for $l < L$ where $e_{L,0} = y - W_L v_{L-1,0} =: \delta_L$. To keep the notation concise, we set $M_L = 1$ in this proof. A generalization for $M_L = \Theta(1)$ is possible. Next, we define

$$\delta_{l < L} := \partial f / \partial u_l. \quad (\text{S.12})$$

Note that a batch gradient can be used with N training samples where $N = O(1)$. One can regard v_l as an $M \times N$ matrix in the derivation.

Using

$$v_{l,1} - v_{l,0} = - \prod_{i=l+1}^L \gamma_i \delta_l, \quad (\text{S.13})$$

we have

$$e_{l,1} := v_{l,1} - \phi(W_l v_{l-1,1}) \quad (\text{S.14})$$

$$= (u_{l,0} - \prod_{i=l+1}^L \gamma_i \delta_l) - \phi(W_l (u_{l-1,0} - \prod_{i=l}^L \gamma_i \delta_{l-1})) \quad (\text{S.15})$$

for $l = 1, \dots, L-1$. Recall that $v_{l,0} = u_{l,0}$ for F-ini. For $l = L$,

$$e_{L,1} := y - W_L h_{L-1,1} \quad (\text{S.16})$$

$$= y - W_L \phi(u_{L-1,0} - \gamma_L \delta_{L-1} \text{diag}(\delta_L)) \quad (\text{S.17})$$

where $\text{diag}(x)$ denotes a diagonal matrix whose diagonal entries are given by x . The above equation comes from

$$v_{L-1,1} = u_{L-1,0} - \frac{\gamma_L}{2} \nabla_{v_{L-1}} \|y - W_L h_{L-1}\|^2 \quad (\text{S.18})$$

$$= u_{L-1,0} - \gamma_L \phi'_{L-1} \circ W_L^\top \delta_L = u_{L-1,0} - \gamma_L \delta_{L-1} \text{diag}(\delta_L). \quad (\text{S.19})$$

The first one-step update of the weight is expressed as

$$\Delta W_{l,1} = \frac{\eta'}{M^{2a_l+c_l}} e_{l,1} h_{l-1,1}^\top, \quad (\text{S.20})$$

In PC, in addition to the usual learning rate η , there also exists γ . Therefore, in addition to the infinitesimal update of the learning rate η for the weight update, we also consider the infinitesimal inference step size γ_L . By applying the perturbation of γ_L to Conditions A.1 and A.2, we derive

$$\Delta U_l + \partial_{\gamma'_L} \Delta U_l|_{\gamma'_L=0} \gamma'_L = \Theta(1), \quad (\text{S.21})$$

$$\Delta V_L + \partial_{\gamma'_L} \Delta V_L|_{\gamma'_L=0} \gamma'_L = \Theta(1) \quad (\text{S.22})$$

where we define

$$\Delta U_l := \partial_{\eta'} \Delta W_{l,1} h_{l-1,s=1}|_{\eta'=0}, \quad (\text{S.23})$$

$$\Delta V_L := \partial_{\eta'} W_{L,0} \Delta h_{l-1,s=1}|_{\eta'=0}. \quad (\text{S.24})$$

It is noteworthy that we retain the zero-th order terms, namely, ΔU_l and ΔV_l in the conditions. This is because, even without the inference phase, parameter updates can progress while the internal states remain at their initialization. Therefore, even if the maximalization of the order is less than $\Theta(1)$ in the first-order perturbation terms, stable learning can still occur. Since μP aims to maximize the order of updates as much as possible, we require the first-order terms of Eqs. (S.21, S.22) to be $\Theta(1)$ whenever possible.

We introduce the following kernel matrix:

$$K_l^A := h_l^\top h_l / M. \quad (\text{S.25})$$

For the random initialization W_l , from Eq. (S.6), we asymptotically obtain

$$K_l^A = \Theta(1), \quad K_L^A = \Theta(1/M^{2(a_L+b_L)}) \quad (\text{S.26})$$

in the infinite-width limit [Yang, 2020].

On Condition A.1.

(i) Case of $1 < l < L$.

$$\partial_{\gamma'_L} \Delta U_l|_{\gamma'_L=0} = \partial \left(\frac{1}{M^{\theta_l}} e_{l,s=1} h_{l-1,s=1}^\top h_{l-1,s=1} \right) \Big|_{\gamma'_L=0} \quad (\text{S.27})$$

$$\begin{aligned} &= \frac{1}{M^{\theta_l}} \partial(e_{l,s=1}) h_{l-1,s=1}^\top h_{l-1,s=1} \Big|_{\gamma'_L=0} + \frac{1}{M^{\theta_l}} e_{l,s=1} \partial(h_{l-1,s=1}^\top h_{l-1,s=1}) \Big|_{\gamma'_L=0} \\ &= \frac{1}{M^{\theta_l}} \partial(e_{l,s=1}) \Big|_{\gamma'_L=0} h_{l-1,s=0}^\top h_{l-1,s=0} \end{aligned} \quad (\text{S.28})$$

$$= \frac{1}{M^{\theta_l + \bar{\gamma}_L - 1}} (-\delta_l + \phi'(W_l u_{l-1,0}) \circ W_l \delta_{l-1}) K_{l-1}^A \quad (\text{S.29})$$

where we used $e_{l < L, s=1}|_{\gamma'_L=0} = 0$ and $h_{l,s=1}|_{\gamma'_L=0} = h_{l,s=0}$. Since $\delta_{l < L} = \Theta(W_L) = \Theta(1/M^{a_L+b_L})$ and $\Delta U_l \sim M^{\theta_l+a_L+b_L-1}$, we have

$$\Delta U_l + \partial_{\gamma'_L} \Delta U_l|_{\gamma'_L=0} \gamma'_L \sim 1/M^{\min\{\theta_l+a_L+b_L-1, \theta_l+\bar{\gamma}_L+a_L+b_L-1\}}. \quad (\text{S.30})$$

The similarity symbol (“ \sim ”) denotes that the left-hand side is of the same order as the right-hand side. Note that if the first-order term becomes negligible, the contribution of the inference phase disappears in the parameter update. To maximize the order of the first-order term, we require

$$\bar{\gamma}_L \leq 0 \quad (\text{S.31})$$

and obtain

$$r_l = \theta_l + \bar{\gamma}_L + a_L + b_L - 1. \quad (\text{S.32})$$

(ii) Case of $l = 1$.

$$\partial_{\gamma'_L} \Delta U_l|_{\gamma'_L=0} = -\frac{1}{M^{\theta_l + \bar{\gamma}_L}} \delta_l K_0^A. \quad (\text{S.33})$$

$$\sim 1/M^{\theta_1 + \bar{\gamma}_L + a_L + b_L} \quad (\text{S.34})$$

Here, we used $e_{l < L, s=1}|_{\gamma'_L=0} = 0$ and $h_{l,s=1}|_{\gamma'_L=0} = h_{l,s=0}$. Similar to the case of $1 < l < L$, Condition (S.21) leads to $\bar{\gamma} \leq 0$ and

$$r_l = \theta_1 + \bar{\gamma}_L + a_L + b_L. \quad (\text{S.35})$$

(iii) Case of $l = L$.

$$\partial_{\gamma'_L} \Delta U_L|_{\gamma'_L=0} \quad (\text{S.36})$$

$$= \frac{1}{M^{\theta_L}} \partial(e_{L,s=1}) h_{L-1,s=1}^\top h_{L-1,s=1} \Big|_{\gamma'_L=0} + \frac{1}{M^{\theta_L}} e_{L,s=1} \partial(h_{L-1,s=1}^\top h_{L-1,s=1}) \Big|_{\gamma'_L=0} \quad (\text{S.37})$$

$$= \frac{1}{M^{\theta_L}} \partial(e_{L,s=1}) \Big|_{\gamma'_L=0} h_{L-1,s=0}^\top h_{L-1,s=0} + \frac{1}{M^{\theta_L}} e_{L,s=1} \partial(h_{L-1,s=1}^\top h_{L-1,s=1}) \Big|_{\gamma'_L=0} \quad (\text{S.38})$$

$$= \frac{1}{M^{\theta_L + \bar{\gamma}_L - 1}} \phi'(W_L u_{L-1,0}) \circ W_L \delta_{L-1} K_{L-1}^A + \frac{1}{M^{\theta_L}} \delta_L \partial(h_{L-1,s=1}^\top h_{L-1,s=1}) \Big|_{\gamma'_L=0} \quad (\text{S.39})$$

$$= \frac{1}{M^{\theta_L + \bar{\gamma}_L - 1}} \phi'(W_L u_{L-1,0}) \circ W_L \delta_{L-1} K_{L-1}^A + \frac{2}{M^{\theta_L}} \delta_L h_{L-1,s=1}^\top \partial(h_{L-1,s=1}) \Big|_{\gamma'_L=0} \quad (\text{S.40})$$

Note that from Eq. (S.17), we have

$$e_{L,s=1}|_{\gamma'_L=0} = -(W_L(\phi'_{L-1} \circ \delta_{L-1})) \circ \delta_L / M^{\bar{\gamma}_L}. \quad (\text{S.41})$$

Since $e_{L,s=1}|_{\gamma'_L=0} = \delta_L \neq 0$,

$$W_L(\phi'_{L-1} \circ \delta_{L-1}) \circ \delta_L = \Theta(1/M^{2(a_L+b_L)-1}). \quad (\text{S.42})$$

For the second term in Eq. (S.40), we have

$$h_{L-1,s=1}^\top \partial(h_{L-1,s=1})|_{\gamma'_L=0} = h_{L-1,s=0}^\top \partial \phi(W_{L-1} v_{L-2,1})|_{\gamma'_L=0} \quad (\text{S.43})$$

$$= h_{L-1}^\top (\phi'_{L-1} \circ W_{L-1} \partial v_{L-2,1})|_{\gamma'_L=0} \quad (\text{S.44})$$

$$= -\frac{\gamma_{L-1}}{M^{\bar{\gamma}_L}} h_{L-1}^\top (\phi'_{L-1} \circ W_{L-1} \delta_{L-2}) \quad (\text{S.45})$$

where we used $v_{L-2,1} - v_{L-2,0} = -\gamma_{L-1} \gamma_L \delta_{L-2}$ from Eq. (S.13). Let us recall that a variable without an index indicates the initial state at $s = 0$. The variable δ_{L-1} includes W_L whereas h_{L-1} is independent of it. Therefore, by applying the CLT with respect to W_L , we have

$$h_{L-1,s=1}^\top \partial(h_{L-1,s=1})|_{\gamma'_L=0} \sim 1/M^{\bar{\gamma}_L+a_L+b_L-1/2}. \quad (\text{S.46})$$

Then,

$$\partial_{\gamma'_L} \Delta U_L|_{\gamma'=0} \sim 1/M^{\min\{\theta_L+\bar{\gamma}_L+2(a_L+b_L)-2, \theta_L+\bar{\gamma}_L+a_L+b_L-1/2\}}. \quad (\text{S.47})$$

In contrast, we have

$$\Delta U_L \sim 1/M^{\theta_L-1}. \quad (\text{S.48})$$

Comparing the zero-th and first order terms (S.47, S.48), we obtain

$$\min\{\theta_L-1, \theta_L+\bar{\gamma}_L+2(a_L+b_L)-2, \theta_L+\bar{\gamma}_L+a_L+b_L-1/2\} = 0 \quad (\text{S.49})$$

Because $a_L + b_L - 1/2 \geq 0$ from Eq. (S.6), we obtain

$$\theta_L - 1 = 0. \quad (\text{S.50})$$

On Condition A.2.

$$\begin{aligned} \partial_{\gamma'_L} \Delta V_L|_{\gamma'_L=0} &= W_{L,0}(\phi'(u_{L-1}) \circ \partial_{\gamma'_L} \partial_{\eta'}(\Delta W_{L-1,1} h_{L-2,1})|_{\eta'=0, \gamma'_L=0}) \\ &= e_M(\delta_{L-1} \circ \frac{1}{M^{\theta_{L-1}}} \partial_{\gamma'}(\Delta W_{L-1} h_{L-2})|_{\gamma'_L=0}) \end{aligned} \quad (\text{S.51})$$

$$= \Theta(1/M^{a_L+b_L+r_{L-1}-1}) \quad (\text{S.52})$$

where e_M denotes an M -dimensional vector with all entries equal to 1. Note that the product with e_M means the summation over M .

Finally, from Conditions 1 and 2, the μP is given by

$$\theta_1 + \bar{\gamma}_L + a_L + b_L = 0 \quad (l = 1), \quad (\text{S.53})$$

$$\theta_l + \bar{\gamma}_L + a_L + b_L - 1 = 0 \quad (1 < l < L), \quad (\text{S.54})$$

$$\theta_L - 1 = 0 \quad (l = L) \quad (\text{S.55})$$

$$a_L + b_L - 1 = 0, \quad (\text{S.56})$$

and $\bar{\gamma}_L \leq 0$. That is,

$$\begin{cases} c_1 = -\bar{\gamma}_L - 1, & c_{1 < l < L} = -\bar{\gamma}_L \geq 0, & c_{l=L} = 1, \\ b_1 = 0, & b_{l > L} = 1/2, & b_l = 1. \end{cases} \quad (\text{S.57})$$

We can also derive the NTK parameterization, which is a commonly used term for the kernel regime for $r_{l < L} = 1/2$ [Yang and Hu, 2021]:

$$\theta_1 + \bar{\gamma}_L + a_L + b_L = 1/2 \quad (l = 1), \quad (\text{S.58})$$

$$\theta_l + \bar{\gamma}_L + a_L + b_L - 1 = 1/2 \quad (1 < l < L), \quad (\text{S.59})$$

$$\theta_L - 1 = 0, \quad (l = L) \quad (\text{S.60})$$

$$a_L + b_L - 1/2 = 0. \quad (\text{S.61})$$

□

It is noteworthy that the gradient computed by Eq. (S.15) differs from δ_l in standard GD, implying that the NTK matrix also deviates from $\nabla_\theta f^\top \nabla_\theta f$. Even in this case, the NTK regime can emerge with a certain modified kernel composed of e_l and h_l . A similar situation arises in the NTK regime of second-order optimization [Karakida and Osawa, 2020]. Although the preconditioner modifies the NTK matrix, the linearization of the model still holds, allowing the emergence of the kernel regime.

A.3 Fixed points of PC in Linear Networks

A.3.1 Proof for Theorem 4.2

In this section, we analyze the fixed point of the inference phase using a linear network:

$$f(x) = W_L W_{L-1} \dots W_1 x. \quad (\text{S.62})$$

Even for linear networks, the properties of the fixed points have rarely been analyzed. An exception is a recent study by [Innocenti et al. \[2024\]](#). They explicitly derived the free energy at a fixed point to analyze the parameter loss landscape of a naive PC. However, their analysis uses an unfolding calculation of a hierarchical Gaussian model to directly derive the free energy. Although this is an elegant derivation, it is not a method for explicitly obtaining the fixed points themselves. Additionally, since their proof is based on $\gamma = 1$, we need another method to determine the dependence on the inference size. Here, we provide a derivation of the states at the fixed point that can be used more generally for various inference sizes and adding a nudge term (in Section A.3.3).

Proof. We consider the inference of naive PC:

$$F(v_1, \dots, v_L) = \frac{\gamma_L}{2} \|y - W_L v_{L-1}\|^2 + \sum_{l=1}^{L-1} \frac{\gamma_l}{2} \|v_l - W_l v_{l-1}\|^2. \quad (\text{S.63})$$

Taking $\frac{\partial F}{\partial v_l} = 0$, we obtain the following fixed-point equations:

$$-\gamma_L W_L^\top (y - W_L v_{L-1}) + \gamma_{L-1} (v_{L-1} - W_{L-1} v_{L-2}) = 0, \quad (l = L) \quad (\text{S.64})$$

$$-\gamma_l W_l^\top (v_l - W_l v_{l-1}) + \gamma_{l-1} (v_{l-1} - W_{l-1} v_{l-2}) = 0, \quad (1 < l < L) \quad (\text{S.65})$$

$$-\gamma_2 W_2^\top (v_2 - W_2 v_1) + \gamma_1 (v_1 - W_1 x) = 0 \quad (l = 1). \quad (\text{S.66})$$

These equations are summarized in the following matrix form:

$$\begin{bmatrix} I & O & \dots & \dots & O \\ -W_L^\top & I & O & \dots & O \\ O & -W_{L-1}^\top & I & \dots & O \\ \vdots & \ddots & \ddots & \ddots & \vdots \\ O & \dots & O & -W_2^\top & I \end{bmatrix} \begin{bmatrix} \gamma_{L-1} e_{L-1}^* \\ \gamma_{L-2} e_{L-2}^* \\ \vdots \\ \gamma_2 e_2^* \\ \gamma_1 e_1^* \end{bmatrix} = \begin{bmatrix} \gamma_L W_L^\top e_L^* \\ O \\ O \\ \vdots \\ O \end{bmatrix} \quad (\text{S.67})$$

where $e_l^* := v_l^* - W_l v_{l-1}^*$ and $e_L^* := y - W_L v_{L-1}^*$.

Here, we use the following lemma:

Lemma A.6. *Define*

$$A_L := \begin{bmatrix} I & O & \dots & \dots & O \\ -W_L^\top & I & O & \dots & O \\ O & -W_{L-1}^\top & I & \dots & O \\ \vdots & \ddots & \ddots & \ddots & \vdots \\ O & \dots & O & -W_2^\top & I \end{bmatrix}. \quad (\text{S.68})$$

Its inverse matrix is given by

$$A_L^{-1} = \begin{bmatrix} I & O & \dots & \dots & O \\ W_L^\top & I & O & \dots & O \\ W_{L-1:L}^\top & W_{L-1}^\top & I & \dots & O \\ \vdots & \ddots & \ddots & \ddots & \vdots \\ W_{2:L}^\top & \dots & W_{2:3}^\top & W_2^\top & I \end{bmatrix}. \quad (\text{S.69})$$

Proof. One can easily derive this inverse matrix. A simple derivation is achieved by induction. We can express

$$A_L = \begin{bmatrix} I & O \\ K & A_{L-1} \end{bmatrix} \quad (\text{S.70})$$

where $K^\top = [W_L, O, \dots, O]$. Suppose that the inverse of A_{L-1} is given by Eq. (S.69). Then,

$$A_L^{-1} = \begin{bmatrix} I & O \\ KA_{L-1}^{-1} & A_{L-1}^{-1} \end{bmatrix}. \quad (\text{S.71})$$

Since $KA_{L-1}^{-1} = [W_L, W_{L-1:L}, \dots, W_{2:L}]^\top$, the inversion of A_L is also given by Eq. (S.69). \square

By using Lemma A.6, we can transform Eq. (S.67) as follows:

$$\begin{bmatrix} e_{L-1}^* \\ e_{L-2}^* \\ \vdots \\ e_2^* \\ e_1^* \end{bmatrix} = \gamma_L \begin{bmatrix} \frac{1}{\gamma_{L-1}} W_L^\top e_L^* \\ \frac{1}{\gamma_{L-2}} W_{L-1:L}^\top e_L^* \\ \vdots \\ \frac{1}{\gamma_2} W_{2:L}^\top e_L^* \end{bmatrix}. \quad (\text{S.72})$$

Although this equation can not be solved explicitly for v_{L-1}^* , we can, nonetheless, solve it by summing over e_l^* as follows:

$$v_{L-1}^* - W_{L-1:1}x \quad (\text{S.73})$$

$$\begin{aligned} &= x e_{L-1}^* + W_{L-1} e_{L-2}^* + \dots + W_{L-1:2} e_1^* \\ &= \gamma_L \left(\frac{1}{\gamma_{L-1}} I + \frac{1}{\gamma_{L-2}} W_{L-1} W_{L-1}^\top + \dots + \frac{1}{\gamma_1} W_{L-1:2} W_{L-1:2}^\top \right) W_L^\top e_L^*. \end{aligned} \quad (\text{S.74})$$

This leads to

$$\begin{aligned} v_{L-1}^* &= \left(I + \frac{\gamma_L}{\gamma_{L-1}} W_L^\top W_L + \frac{\gamma_L}{\gamma_{L-2}} W_{L-1} W_{L-1}^\top W_L^\top W_L + \dots + \frac{\gamma_L}{\gamma_1} W_{L-1:2} W_{L-1:2}^\top W_L^\top W_L \right)^{-1} \\ &\quad \cdot \left(W_{L-1:1}x + \gamma_L \left(\frac{1}{\gamma_{L-1}} I + \frac{1}{\gamma_{L-2}} W_{L-1} W_{L-1}^\top + \dots + \frac{1}{\gamma_1} W_{L-1:2} W_{L-1:2}^\top \right) W_L^\top y \right). \end{aligned} \quad (\text{S.75})$$

Set an $M_L \times M_L$ matrix

$$C_\gamma(W) := \sum_{i=2}^L \frac{\gamma_L}{\gamma_{i-1}} W_{L:i} W_{L:i}^\top. \quad (\text{S.76})$$

Then,

$$e_L^* = y - W_L v_{L-1}^* \quad (\text{S.77})$$

$$\begin{aligned} &= y - (I + C_\gamma(W))^{-1} (W_{L:1}x + (I + C_\gamma(W)) y) \\ &= (I + C_\gamma(W))^{-1} (y - f). \end{aligned} \quad (\text{S.78})$$

Thus, at the fixed point, the local loss is explicitly obtained as

$$e_l^* = \frac{\gamma_L}{\gamma_l} W_{L:l+1}^\top (I + C_\gamma(W))^{-1} (y - f). \quad (\text{S.79})$$

We can also obtain v_l^* . From e_1^* , we have

$$v_1^* = W_1 x + \frac{\gamma_L}{\gamma_1} W_{L:2}^\top (I + C_\gamma(W))^{-1} (y - f). \quad (\text{S.80})$$

By induction, we have

$$v_l^* = e_l^* + W_l v_{l-1}^* \quad (\text{S.81})$$

$$= W_{l:1}x + \left(\frac{\gamma_L}{\gamma_l} W_{L:l+1}^\top + \sum_{i=2}^{l-1} \frac{\gamma_L}{\gamma_{i-1}} W_{l:i} W_{L:i}^\top \right) (I + C_\gamma(W))^{-1} (y - f). \quad (\text{S.82})$$

\square

A.3.2 Balance condition determining $\gamma_{l < L}$

Here, we consider the order of $e_{l,1}$ with respect to $\gamma_{l < L}$. For a linear network with one-shot SI, we obtain

$$e_{l,1} = - \prod_{i=l+1}^L \gamma_i (\delta_l - \gamma_l W_l \delta_{l-1}) \sim 1/M^{\min(0, \bar{\gamma}_l) + \sum_{i=l+1}^L \bar{\gamma}_i} \quad (\text{S.83})$$

In contrast, recall that the order of e_l^* at the fixed point is

$$e_l^* \sim 1/M^{-\bar{\gamma}_l + \min(0, \bar{\gamma}_l)}. \quad (\text{S.84})$$

Therefore, to satisfy $e_{l,1} \sim e_l^*$, the following is necessary:

$$\sum_{i=l+1}^L \bar{\gamma}_i = -\bar{\gamma}_l \quad (\text{S.85})$$

for all $l < L$. This is equivalent to $\bar{\gamma}_l = 0$ for all $l < L$. Thus, $e_{l,1} \sim e_l^*$ holds if and only if $\bar{\gamma}_{l < L} = 0$.

A.3.3 Nudged Predictive Coding

Predictive Coding with a nudge term updates the state v_l and weights W_l to minimize the following free energy function [Alonso et al., 2022, Millidge et al., 2023, Pinchetti et al., 2024]:

$$\mathcal{F} = \beta \mathcal{L}(y, v_L) + \sum_{l=1}^L \gamma_l \frac{1}{2} \|v_l - W_l \phi(v_{l-1})\|^2. \quad (\text{S.86})$$

Here, β is a nudge coefficient parameter that covers some variants of the PC algorithms in the previous work. We can extend Theorem 4.2 to the nudged PC.

Theorem A.7. Suppose an L -layered linear network and put $e_l^* = v_l^* - W_l v_{l-1}^*$, where $*$ denotes the fixed point of the inference given by Eq. (S.86). The following holds:

$$e_l^* = v_l^* - W_l v_{l-1}^* = \frac{\gamma_L}{\gamma_l} W_{L:l+1}^\top \left(I + \frac{\gamma_L}{\beta} I + C_\gamma(W) \right)^{-1} (W_{L:1} x - y) \quad (\text{S.87})$$

$$e_L^* = v_L^* - W_L v_{L-1}^* = \left(I + \frac{\gamma_L}{\beta} I + C_\gamma(W) \right)^{-1} (W_{L:1} x - y) \quad (\text{S.88})$$

where $W_{L:i} = W_L W_{L-1} \dots W_i$.

Proof. Put

$$F(v_1, \dots, v_L) = \beta \|y - v_L\|^2 + \sum_{l=1}^L \frac{\gamma_l}{2} \|v_l - W_l v_{l-1}\|^2. \quad (\text{S.89})$$

Taking $\frac{\partial F}{\partial v_l} = 0$, we have

$$\beta(v_L - y) + \gamma_L(v_L - W_L v_{L-1}) = 0 \quad (\text{S.90})$$

$$-\gamma_l W_l^\top (v_l - W_l v_{l-1}) + \gamma_{l-1}(v_{l-1} - W_{l-1} v_{l-2}) = 0 \quad (1 < l \leq L) \quad (\text{S.91})$$

$$-\gamma_2 W_2^\top (v_2 - W_2 v_1) + \gamma_1(v_1 - W_1 x) = 0 \quad (l = 1). \quad (\text{S.92})$$

Putting $\chi = v_L - y$, the system of equations can be written in a matrix form as follows:

$$\begin{bmatrix} I & O & \dots & \dots & O \\ -W_L^\top & I & O & \dots & O \\ O & -W_{L-1}^\top & I & \dots & O \\ \vdots & \ddots & \ddots & \ddots & \vdots \\ O & \dots & O & -W_2^\top & I \end{bmatrix} \begin{bmatrix} \gamma_L e_L^* \\ \gamma_{L-1} e_{L-1}^* \\ \vdots \\ \gamma_2 e_2^* \\ \gamma_1 e_1^* \end{bmatrix} = \begin{bmatrix} -\beta \chi^* \\ O \\ O \\ \vdots \\ O \end{bmatrix}. \quad (\text{S.93})$$

From Lemma A.6, the above equation is transformed into

$$\begin{bmatrix} e_L^* \\ e_{L-1}^* \\ \vdots \\ e_2^* \\ e_1^* \end{bmatrix} = -\beta \begin{bmatrix} \frac{1}{\gamma_L} \chi^* \\ \frac{1}{\gamma_{L-1}} W_L^\top \chi^* \\ \vdots \\ \frac{1}{\gamma_1} W_{2:L}^\top \chi^* \end{bmatrix}. \quad (\text{S.94})$$

Take the following summation:

$$\begin{aligned} e_L^* + W_L e_{L-1}^* + W_{L-1} e_{L-2}^* + \cdots + W_{L-1:2} e_1^* &= v_L^* - W_{L:1} x \\ &= -\frac{\beta}{\gamma_L} (I + C_\gamma(W)) \chi^*. \end{aligned} \quad (\text{S.95})$$

Thus, we can explicitly obtain v_L as

$$v_L^* = \left(\frac{\beta}{\gamma_L} I + \frac{\beta}{\gamma_L} C_\gamma(W) \right)^{-1} \left(W_{L:1} x + \frac{\beta}{\gamma_L} (I + C_\gamma(W)) y \right). \quad (\text{S.96})$$

Thus, χ can be written as follows:

$$\chi^* = y - v_L^* \quad (\text{S.97})$$

$$= y - \left(\frac{\beta}{\gamma_L} I + \frac{\beta}{\gamma_L} C_\gamma(W) \right)^{-1} \left(W_{L:1} x + \frac{\beta}{\gamma_L} (I + C_\gamma(W)) y \right) \quad (\text{S.98})$$

$$= \left(I + \frac{\beta}{\gamma_L} I + \frac{\beta}{\gamma_L} C_\gamma(W) \right)^{-1} (y - f). \quad (\text{S.99})$$

From the above, we conclude that

$$e_l^* = \frac{\beta}{\gamma_l} W_{L:l+1}^\top \left(I + \frac{\beta}{\gamma_L} I + \frac{\beta}{\gamma_L} C_\gamma(W) \right)^{-1} (y - f) \quad (\text{S.100})$$

$$= \frac{\gamma_L}{\gamma_l} W_{L:l+1}^\top \left(I + \frac{\gamma_L}{\beta} I + C_\gamma(W) \right)^{-1} (y - f) \quad (\text{S.101})$$

at the fixed point. □

A.4 Target Propagation

A.4.1 Derivation of Theorem 5.1.

Assume that the feedback network is linear: $g_l(x) = Q_l x$. Here, we consider a reconstruction loss with L2 regularization:

$$l(Q_{l,s}) = \|Q_{l,s} \phi(W_{l-1} h_{l-1}) - h_{l-1}\|^2 + \mu_l \|Q_{l,s}\|^2 \quad (\text{S.102})$$

with $\mu_l \geq 0$. Note that while some work adds noise to h_{l-1} , it does not affect the order; therefore, we will ignore it in this derivation. As described below, by taking the ridge-less limit of μ , we can evaluate the parameterization of the original TP and Difference Target Propagation (DTP) in a clear and unified manner. Considering the fixed point for Q_L , since $\frac{\partial l(Q_l)}{\partial Q_l} = 0$ holds, we have

$$Q_l^* = h_{l-1} (h_l^\top h_l + \mu_l I)^{-1} h_l^\top \quad (\text{S.103})$$

where $h_l = \phi(W_l h_{l-1})$. The feedback network is given by the network with Eq. (S.103). As a side note, this weight is essentially the same as the pseudo-inverse weight, which is known as an extension of the Hebbian weight [Kanter and Sompolinsky, 1987].

Local targets of DTP. DTP is an improved methods of TP, where \hat{h}_L is propagated as follows:

$$\hat{h}_i = g_i^{\text{diff}}(\hat{h}_{i+1}, h_{i+1}, h_i) = g_i(\hat{h}_{i+1}) - (g_i(h_{i+1}) - h_i). \quad (\text{S.104})$$

For the last layer, the error is given by

$$\hat{h}_L = h_L + \beta(y - h_L) \quad (\text{S.105})$$

For a linear feedback network, we have

$$\hat{h}_l = g_{l+1}(\hat{h}_{l+1}) - (g_l(h_{l+1}) - h_l) \quad (\text{S.106})$$

$$= h_l + Q_{l+1}(\hat{h}_{l+1} - h_{l+1}) \quad (\text{S.107})$$

$$= h_l + Q_{l+1}((h_{l+1} + Q_{l+2}(\hat{h}_{l+2} - h_{l+2})) - h_{l+1}) \quad (\text{S.108})$$

$$= h_l + Q_{l+1}Q_{l+2}(\hat{h}_{l+2} - h_{l+2}) \quad (\text{S.109})$$

$$= h_l - \beta \prod_{i=l+1}^L Q_i \delta_L. \quad (\text{S.110})$$

Therefore, at the equilibrium point for Q_l , for $l \leq L-1$, we have

$$\hat{h}_l - h_l = -\beta \prod_{i=l+1}^L Q_i^* \delta_L \quad (\text{S.111})$$

$$= -\beta h_l \prod_{i=l+1}^{L-1} (h_i^\top h_i + \mu_i I)^{-1} h_i^\top h_i (h_L^\top h_L + \mu_L I)^{-1} h_L^\top \delta_L \quad (\text{S.112})$$

$$= -\beta h_l \prod_{i=l+1}^{L-1} (K_i^A + \mu'_i I)^{-1} K_i^A (K_L^A + \mu'_L I)^{-1} h_L^\top \delta_L \quad (\text{S.113})$$

where $\delta_L = \partial \mathcal{L} / \partial f$. To avoid an uninteresting change of order, we introduce $\mu_l = \mu'_l / M^{\bar{\mu}_l}$ and require that it have the same order as K_l^A . This is essentially equivalent to the valid condition argued in [Ishikawa and Karakida \[2024\]](#), which requires the damping term to have the same order as the preconditioner in the second-order optimization. We note that we can take the ridge-less limit $\mu'_l \rightarrow 0+$ because K_l^A (S.26) is typically set to be regular at random initialization in the neural tangent kernel literature [[Jacot et al., 2018](#), [Yang, 2020](#)]. For instance, this holds true for normalized input samples with $\|x\| = 1$.

Local targets of original TP. The signal propagation in the feedback network is

$$\hat{h}_l = Q_l^* \cdots Q_L^* \hat{h}_L \quad (\text{S.114})$$

$$= h_l \prod_{i=l+1}^{L-1} (h_i^\top h_i + \mu_i I)^{-1} h_i^\top h_i (h_L^\top h_L + \mu_L I)^{-1} h_L^\top (h_L - \beta \delta_L) \quad (\text{S.115})$$

$$\rightarrow h_l - \beta h_l \prod_{i=l+1}^{L-1} (K_i^A)^{-1} K_i^A (K_L^A)^{-1} h_L^\top \delta_L \quad (\mu'_l \rightarrow 0+). \quad (\text{S.116})$$

Thus, the target is reduced to essentially the same as that in DTP (S.113) and we can treat both in the same manner.

On Condition A.1.

$$\partial_{\eta'} \Delta W_{L-1} h_{L-2,1} \big|_{\eta'=0} = \frac{1}{M^{\theta_{L-1}}} (\hat{h}_{L-1} - h_{L-1}) h_{L-1}^\top h_{L-1} \quad (\text{S.117})$$

$$= -\frac{1}{M^{\theta_{L-1}-1}} \beta h_{L-1} (h_L^\top h_L + \mu_L I)^{-1} h_L^\top \delta_L K_{L-1}^A \quad (\text{S.118})$$

$$= -\frac{1}{M^{\theta_{L-1}-1}} \beta h_{L-1} (K^A + \mu'_L I)^{-1} (K^A - M^{-1} h_L^\top y) K_{L-1}^A. \quad (\text{S.119})$$

Similarly, when $\hat{h}_l - h_l = -\beta \prod_{i=l+1}^L Q_i \delta_L$, we have

$$\partial_{\eta'} \Delta W_l h_{l-1,1} \big|_{\eta'=0} = \frac{1}{M^{\theta_l}} (\hat{h}_l - h_l) h_{l-1}^\top h_{l-1} \quad (\text{S.120})$$

$$= -\frac{1}{M^{\theta_{l-1}}} \beta h_l \prod_{i=l+1}^L (h_i^\top h_i + \mu_i I)^{-1} h_i^\top h_i (h_L^\top h_L + \mu_L I)^{-1} h_L^\top \delta_L K_{l-1}^A \quad (\text{S.121})$$

$$= -\frac{1}{M^{\theta_{l-1}}} \beta h_l \prod_{i=l+1}^L (K_i^A + \mu'_i I)^{-1} K_i^A (K_L^A + \mu'_L I)^{-1} (K_L^A - M^{-1} h_L^\top y) K_{l-1}^A \quad (\text{S.122})$$

for $l = 1, \dots, L-2$. On the right-hand side, $h_L \sim 1/M^{a_L+b_L-1/2}$, and from Eq. (S.26), we have

$$K_L^A - M^{-1} h_L^\top y \sim \max\{1/M^{2(a_L+b_L)}, 1/M^{a_L+b_L+1/2}\} \quad (\text{S.123})$$

$$= 1/M^{a_L+b_L+1/2}. \quad (\text{S.124})$$

In the last line, we used $a_L + b_L \geq 1/2$. Here, from Assumption A.4, which states that $a_L + b_L \geq 1/2$, we obtain

$$r_l = \begin{cases} \theta_1 - a_L - b_L + 1/2 & (l=1), \\ \theta_l - 1 - a_L - b_L + 1/2 & (1 < l < L), \\ \theta_L - 1 & (l=L). \end{cases} \quad (\text{S.125})$$

On Condition A.2.

$$\partial_{\eta'} (W_{L,0} \Delta h_{L-1,1}) \big|_{\eta'=0} = \frac{1}{M^{\theta_{L-1}}} W_{L,0} (\hat{h}_{L-1} - h_{L-1}) h_{L-1}^\top \quad (\text{S.126})$$

$$= -\frac{1}{M^{\theta_{L-1}-1}} \beta h_L (h_L^\top h_L + \mu'_L I)^{-1} h_L^\top \delta_L K_{L-1}^A \quad (\text{S.127})$$

$$= -\frac{1}{M^{\theta_{L-1}-1}} \beta h_L (K_L^A + \mu'_L I)^{-1} (K_L^A - M^{-1} h_L^\top y) K_{L-1}^A. \quad (\text{S.128})$$

Thus, its order is

$$\partial_{\eta'} (W_{L,0} \Delta h_{L-1,1}) \big|_{\eta'=0} \sim 1/M^{\theta_{L-1}-1+(a_L+b_L-1/2)-2(a_L+b_L)+(a_L+b_L+1/2)} \quad (\text{S.129})$$

$$= 1/M^{\theta_{L-1}-1=r_{L-1}+(a_L+b_L)-1/2}. \quad (\text{S.130})$$

Finally, from Conditions A.1 and A.2, the μP is given by

$$\theta_1 - a_L - b_L + 1/2 = 0 \quad (l=1), \quad (\text{S.131})$$

$$\theta_l - a_L - b_L - 1/2 = 0 \quad (1 < l < L), \quad (\text{S.132})$$

$$\theta_L - 1 = 0 \quad (l=L), \quad (\text{S.133})$$

$$a_L + b_L - 1/2 = 0. \quad (\text{S.134})$$

□

A.4.2 Disappearance of Kernel regime

Corollary A.8. *Stable learning satisfying Condition A.2 leads to $r_{L-1} = 0$ for TP and DTP.*

Proof. From Eq. (S.130), we have

$$r_{L-1} + (a_L + b_L) - 1/2 = 0. \quad (\text{S.135})$$

From Eq. (S.6), $a_L + b_L \geq 1/2$ and we have $r_{L-1} \geq 0$. In contrast, from the stability of learning, we have $r_{L-1} \leq 0$. Thus, $r_{L-1} = 0$. □

Note that, precisely speaking, $r_{L-1} = 0$ does not necessarily imply $r_{l < L-1} = 0$. However, it is often considered unnatural (or uninteresting) to examine cases in which the progress of learning depends on

individual layers. Therefore, the μP typically assumes a uniform parameterization, meaning $r_{l < L} = r$ (see Theorem G.4 of Yang and Hu [2021]). In this sense, $r_{L-1} = 0$ indicates the disappearance of the kernel regime.

One might be surprised by the fact that $b_L = 1/2$ is allowed in the feature learning and that the kernel regime disappears. Note that the feedback weight in the last layer (S.103) essentially differs from W_L . The feedback weight receives h_L as input whereas W_l receives h_{L-1} . This makes

$$Q_L \sim 1/M^{1/2-(a_L+b_L)} \quad (\text{S.136})$$

$W_L \sim 1/M^{a_L+b_L}$. The gradient is proportional to Q_L in TP and W_L in BP. The feedback weight contributes more significantly to TP's gradient when $a_L + b_L \geq 1/2$. This eventually makes the index r of the hidden layer (S.125) get quite large even for $a_L + b_L = 1/2$. We also need to be careful about the order of condition A.2 (S.130). Because the feedback weight (S.103) has a lower alignment exponent [Everett et al., 2024], this causes the condition 2 of TP to be smaller than that of SGD (or K-FAC), i.e., $1/M^{r_{L-1}+(a_L+b_L)-1}$. Therefore, the stable feature learning is possible even for $a_L + b_L = 1/2$.

Remark on zero head initialization. Related to the size of b_L , the parameter initialization with $b_L > 1/2$ ($b_L > 1$ for SGD) reduces to the μP of $b_L = 1/2$ ($b_L = 1$ for SGD) because $W_{l,0}$ becomes negligible compared to $\Delta W_{l,0}$. To illustrate the intuition, let us introduce the case where the weight of the last layer in a feedforward network is initialized as $W_L = O$, that is, $b_L = \infty$.

In this case, only the last layer is updated during the first step because $Q_L^* = O$ does not propagate the local error to the downstream layers. After the first-step update, the weight is given by

$$W_{L,1} = -\frac{\eta'}{M^{\theta_L}} \delta_L h_{L-1}^\top. \quad (\text{S.137})$$

and $W_{l < L,1} = W_{l < L,0}$. Thus,

$$\partial_{\eta'} \Delta W_l h_{l-1,1} \big|_{\eta'=0} = -\frac{1}{M^{\theta_L}} \delta_L h_{L-1}^\top h_{L-1} \quad (\text{S.138})$$

$$= -\frac{1}{M^{\theta_{L-1}}} \delta_L K_{L-1}^A. \quad (\text{S.139})$$

and

$$h_{L,1} = \Theta(1/M^{\theta_L-1}), \quad K_L^A = \Theta(1/M^{2\theta_L-1}), \quad (\text{S.140})$$

Substituting these into Eqs. (S.119, S.122), we obtain

$$r_l = \begin{cases} \theta_1 - \theta_L + 1 & (l = 1), \\ \theta_l - \theta_L & (1 < l < L), \\ \theta_L - 1 & (l = L). \end{cases} \quad (\text{S.141})$$

From Eq. (S.128),

$$\partial_{\eta'} (W_{L,0} \Delta h_{L-1,1}) \big|_{\eta'=0} = \Theta(1/M^{\theta_{L-1}-1}). \quad (\text{S.142})$$

Finally, Conditions A.1 and A.2 lead to

$$\theta_1 - (\theta_L - 1) = 0 \quad (l = 1), \quad (\text{S.143})$$

$$\theta_l - 1 - (\theta_L - 1) = 0 \quad (1 < l < L), \quad (\text{S.144})$$

$$\theta_L - 1 = 0 \quad (\text{S.145})$$

Thus, the μP is the same as in the case of random head initialization.

A.5 Stable parametrization for feedback network

The feedback network minimizes the following loss function:

$$L(Q_l) = \frac{1}{2M_{l-1}} \|\phi(Q_l h_l) - h_{l-1}\|^2. \quad (\text{S.146})$$

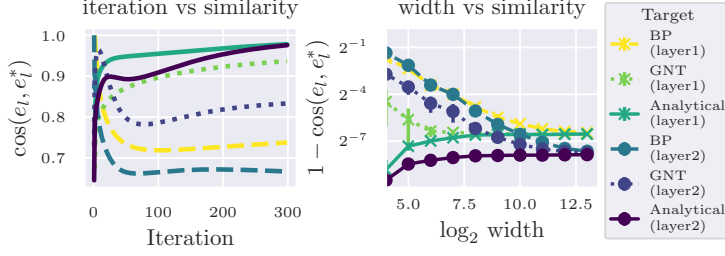


Figure S.1 : During training of the linear network, it converges to the analytical solution. We trained a 3-layer linear network using synthetic data.

where dividing by M_{L-1} is to ensure that $L(Q_l) = \Theta(1)$, which is the default setting in PyTorch. We consider the parametrization in the feedback network:

$$Q_l \sim \mathcal{N}(0, \sigma'^2 / M^{2\bar{q}_l}), \quad \tau_l = \frac{\tau'_l}{M^{\bar{\tau}_l}}, \quad (\text{S.147})$$

where τ_l denotes the learning rate for the feedback network.

To ensure that the update $\Delta Q_l h_l = \Theta(1)$ holds, we have

$$\Delta Q_l h_l = \frac{\tau'}{M^{\bar{\tau}_l+1}} (\phi(Q_l h_l) - h_{l-1}) \phi'(Q_l h_l) h_l^\top h_l. \quad (\text{S.148})$$

Here, because $h_{l<L}^\top h_{l<L} = \Theta(M)$ and $h_L^\top h_L = \Theta(1/M^{2b_L-1})$, assuming $\Delta Q_l h_l = \Theta(1/M^{r_l})$, we obtain:

$$r_l = \begin{cases} \bar{\tau}_l & (1 < l < L), \\ \bar{\tau}_L + 2b_L & (l = L) \end{cases} \quad (\text{S.149})$$

Therefore,

$$\bar{\tau}_{l<L} = 0, \quad \bar{\tau}_L = -2b_L. \quad (\text{S.150})$$

If we optimize the feedback network for one step, we have

$$Q_{l<L,1} = Q_{l<L,0} - \frac{\tau'}{M^{\bar{\tau}_l+1}} h_{l-1} h_l^\top \sim \frac{1}{M^{\min(1, q_l)}}, \quad (\text{S.151})$$

$$Q_{L,1} = Q_{L,0} - \frac{\tau'}{M^{\bar{\tau}_L+1}} h_{L-1} h_L^\top \sim \frac{1}{M^{\min(1/2-b_L, q_L)}}. \quad (\text{S.152})$$

And,

$$Q_{l<L}^* = h_{l-1} (h_l^\top h_l + \mu I)^{-1} h_l^\top \sim \frac{1}{M}, \quad (\text{S.153})$$

$$Q_L^* = h_{L-1} (h_L^\top h_L + \mu I)^{-1} h_L^\top \sim \frac{1}{M^{1/2-b_L}}. \quad (\text{S.154})$$

Therefore, in this case, $Q_{l,1} = Q_l^*$ holds when

$$\bar{q}_{l<L} \geq 1, \quad \bar{q}_L \geq 1/2 - b_L. \quad (\text{S.155})$$

B Additional Experiments

B.1 Predictive Coding

B.1.1 Linear Network

In Figure S.1, we measure the similarity of the inference vector with BP, GNT, and the analytical solution. With fewer inference iterations, the model behaves more like BP; however, as the number of iterations increases, the model converges toward the analytical solution. Furthermore, as the middle layer width M_l increases, the gap between GNT and BP decreases. Figure S.2 further demonstrates that reducing the output dimension M_L brings the model closer to BP. However, increasing M_L moves the model away from BP, though this divergence is more gradual as $\bar{\gamma}_L$ approaches zero.

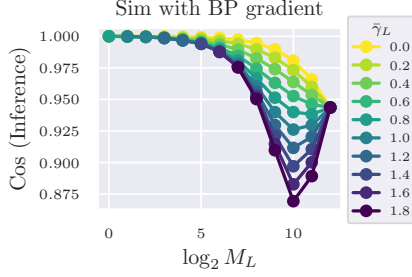


Figure S.2 : As M_L approaches 1, the update vector in PC converges to that of BP. We conducted inference training on a 3-layer linear network and measured the similarity between PC and BP. The results demonstrate that PC approaches BP as M_L decreases and $\bar{\gamma}_L$ increases.

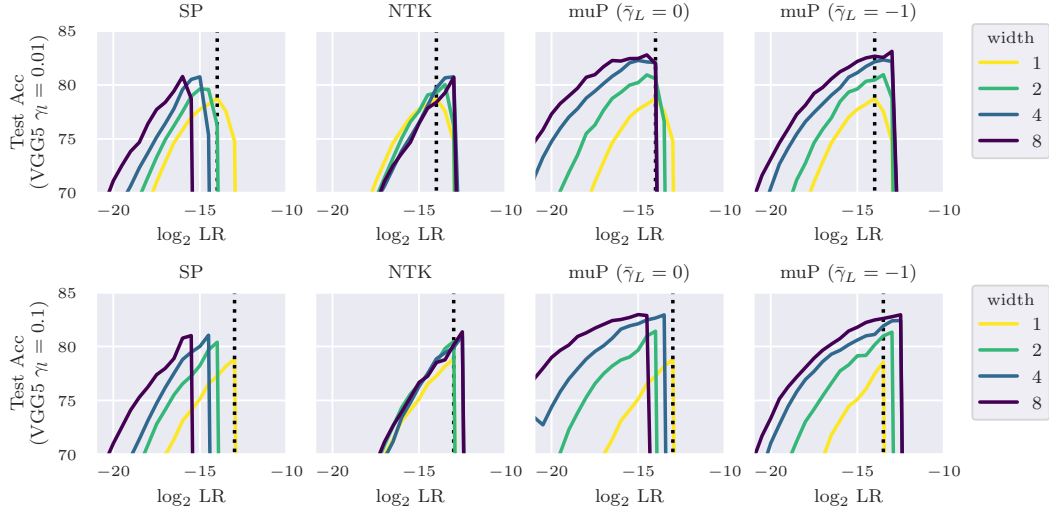


Figure S.3 : In VGG5, the learning rate also transfers across widths. In SP, the optimal learning rate shifts based on model width, whereas in μP , it remains fixed. Additionally, we trained with two different γ_l values, and under μP ($\bar{\gamma}_L = -1$), the learning rate consistently transfers across widths, regardless of γ_l . The model was trained for 40 epochs on 1024 samples from FashionMNIST.

B.1.2 Additional Experiments on μ transfer for PC

Architecture In the main text, we primarily focused on MLP and CNN. However, our μP is architecture-independent. The results for VGG5 are presented in Figure S.3 . Furthermore, the μ Transfer observed in Figure 4 also holds for MLP, as demonstrated in Figure S.4 .

Loss Type In the main text, we mainly used MSE loss. However, this can be replaced with cross-entropy (CE) loss. As demonstrated in Figure S.5 , μP for PC also transfers the learning rate across widths when using cross-entropy loss.

Optimizer In this paper, we primarily focus on weight updates using SGD. However, it is also possible to update the weights using Adam instead of SGD. In this case, the corresponding μP is as follows:

$$\begin{cases} b_1 = 0, & b_{l>1} = 1/2, & b_L = 1, \\ c_1 = 0, & c_{l>1} = 1. \end{cases} \quad (\text{S.156})$$

For Adam, the scaling of b_l and c_l does not depend on $\bar{\gamma}_L$. Additionally, in Adam, the gradients are normalized, which means that μP remains unchanged regardless of whether the gradients are generated by BP or PC. When considering the stability of the inference, scaling with respect to $\bar{\gamma}_L$ can be treated in the same manner as in the case of SGD.

$$\bar{\gamma}_{l<L} = 0, \quad \bar{\gamma}_L = 1. \quad (\text{S.157})$$

Train sample We reduced the number of training samples in most of the graphs for μ Transfer. By reducing the number of training samples, finite-width models are known to behave more similarly to

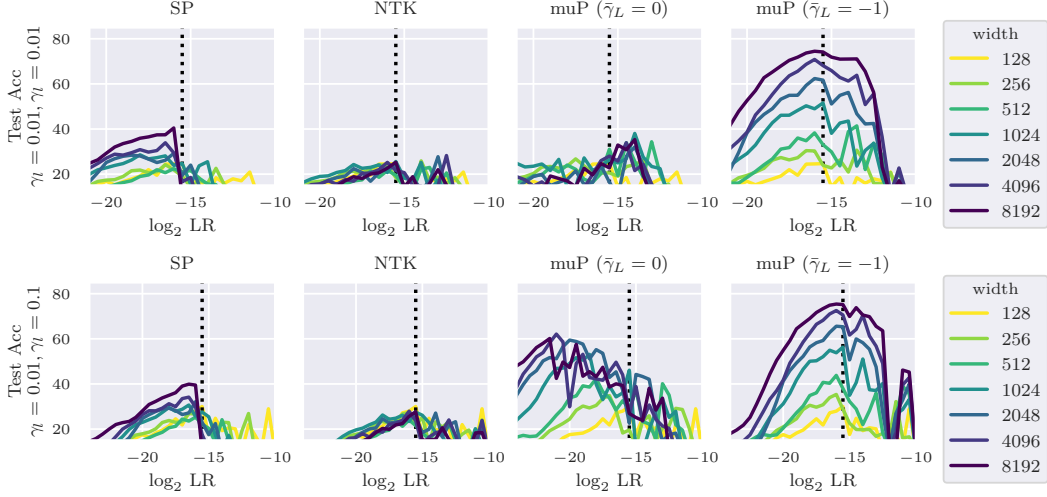


Figure S.4 : **Without F-ini, μP with $\bar{\gamma}_L = -1$ transfers the learning rates across width also in MLP.** We trained 3-layer MLP on FashionMNIST without F-ini.

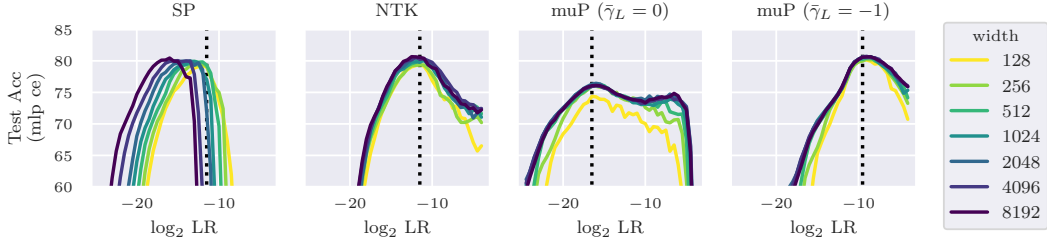


Figure S.5 : **μP for PC transfers learning rates across widths even with Cross Entropy.** We train 3-layer MLP for 40 epochs on 1024 samples from FashionMNIST.

infinite-width models, as has often been seen in papers examining the theoretical aspects of feature learning [Geiger et al., 2020, Ishikawa and Karakida, 2024]. However, even when training on the full dataset, μP remains stable across widths, as shown in Figure S.8 .

Inference Loss When considering the stability of inference, we can observe the loss before updating the parameters after inference. As shown in Figure S.9 , when training a 3-layer MLP on FashionMNIST, only μP with $\bar{\gamma}_L = -1$ consistently reduces the inference loss as the model width increases.”

Base width and inference iterations In μ -transfer, some research set the width of the smaller model used for tuning the learning rate, as the base width, denoted by M' , and adjusts the learning rate using $\eta_l = \eta'_l / (M/M')^{\alpha}$. As shown in Figure S.10 , the choice of M' (a smaller M') can sometimes make μP with $\bar{\gamma}_L = 0$ more sensitive.

As shown in Figure S.11 , the shift in the optimal learning rate at $\gamma_L = 0$ with $M' = 128$ becomes more evident as the number of inference iterations increases. This is likely because with more iterations, the dynamics of inference play a more critical role in weight updates. In summary, to achieve stable μ Transfer independent of the base width and the number of inference iterations, we should use μP with $\gamma_L = -1$.

Sequential Inference and Synchronous Inference In the main text, we focused on Sequential Inference, where u_l is updated layer by layer, starting from the output layer. However, Synchronous Inference, where all layers are updated simultaneously, can also be considered. For the differences between Sequential Inference and Synchronous Inference, see Algorithm.1. As shown in Figure S.12 , since μP for PC is validated at fixed points, it is also applicable to Synchronous Inference.

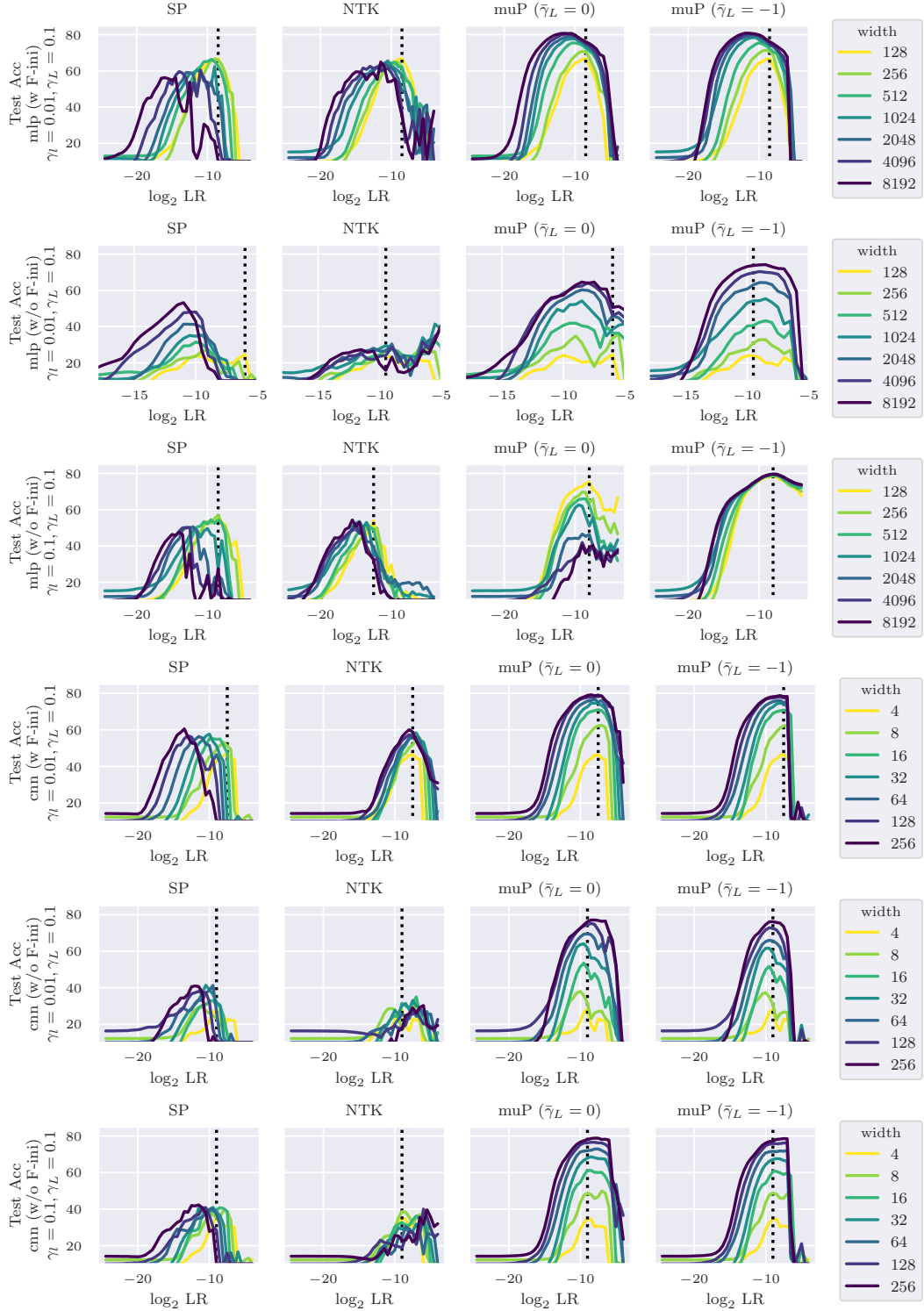


Figure S.6 : μP with $\bar{\gamma}_L = -1$ can constantly transfer the learning rates across width We confirmed μ Transfer when training PC with Adam to update parameters in both MLP and CNN. In the training of MLP without F-ini, we observe that μP with $\bar{\gamma}_L = -1$ consistently stabilizes training and performs well. All experiments were conducted on FashionMNIST with 1024 samples.

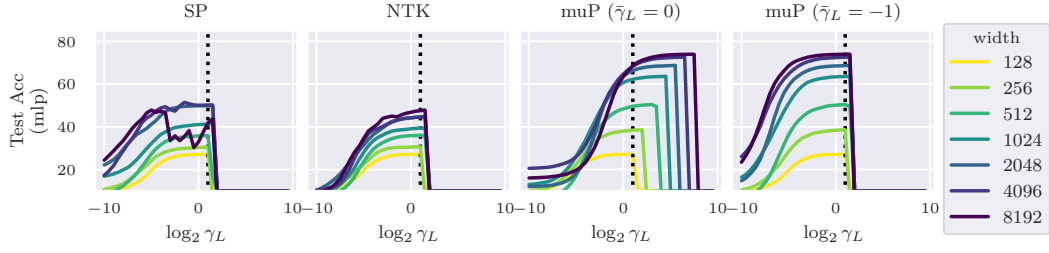


Figure S.7 : When training with Adam, μP with $\bar{\gamma}_L = -1$ transfer γ_L across width. We trained a 3-layer MLP on FashionMNIST with Adam.

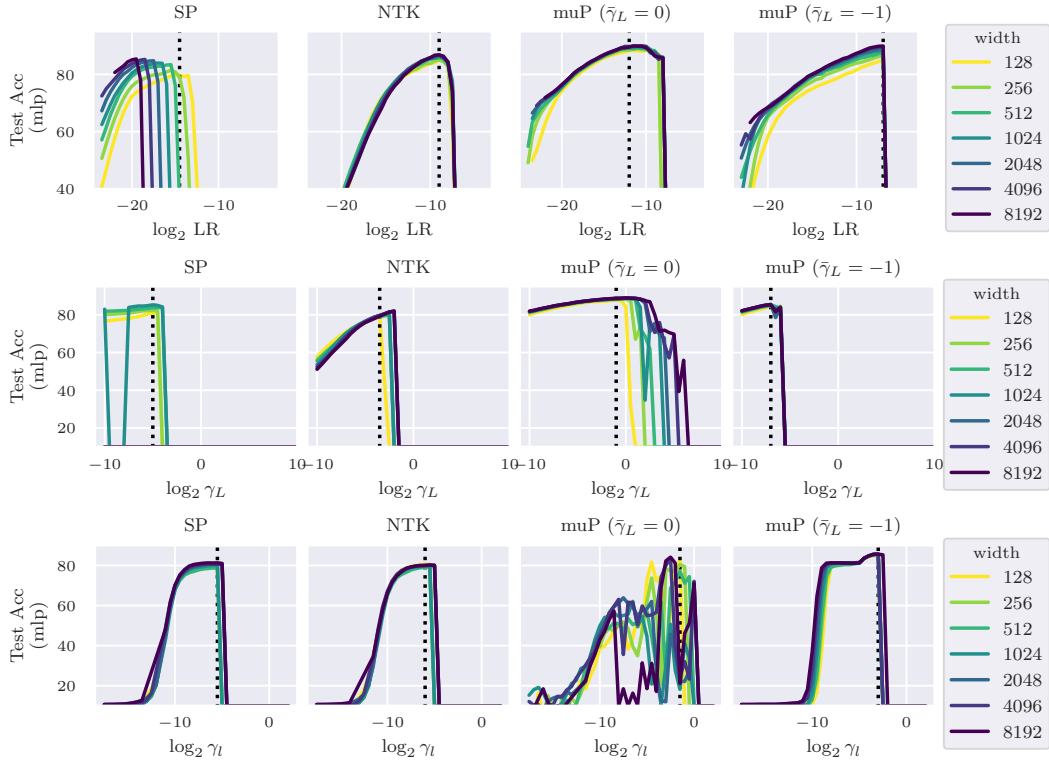


Figure S.8 : The results of μP for PC are independent of the number of training samples. We train 3-layer MLP on FashionMNIST with full training samples. The stability of μP holds even with all training samples.

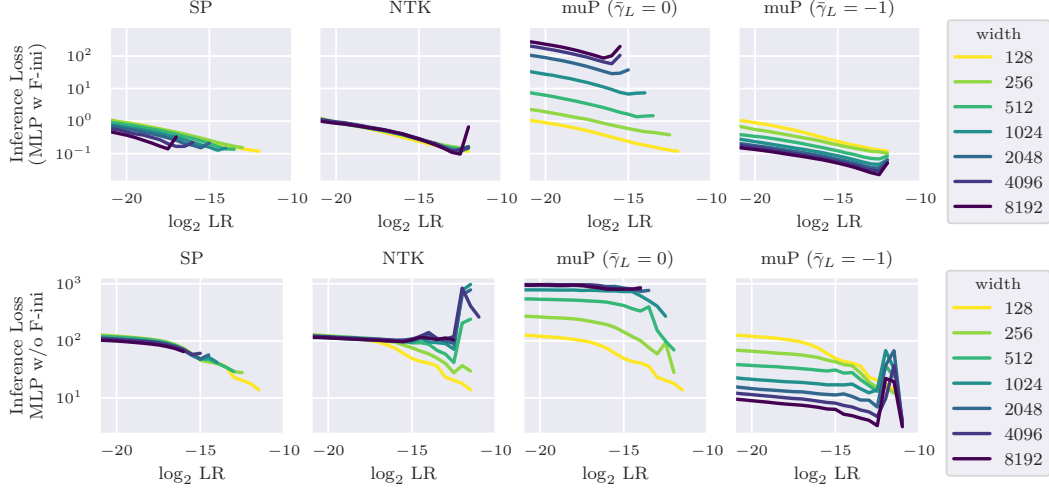


Figure S.9 : **When evaluating the loss after inference, only μP with $\bar{\gamma}_L = -1$ satisfies the empirical rule of “wider is better”** Regardless of whether F-ini is applied, μP with $\bar{\gamma}_L = -1$ consistently reduces the loss during inference with stability. We train 3-layer MLP on FashionMNIST.

Algorithm 1 PC Algorithm (Simultaneous or [Sequential inference](#))

- 1: **for** $s = 1$ to n **do**
 - 2: $e_{L,s} \leftarrow \nabla_{u_{L,s}} \mathcal{L}(W_L \phi_L(u_{L-1,s}), y)$
 - 3: **for** $l = L - 1$ to 1 **do**
 - 4: $e_{l,s} \leftarrow u_{l,s} - W_l \phi_{l-1}(u_{l-1,s})$
 - 5: $e_{l+1,s} \leftarrow u_{l+1,s+1} - W_{l+1} \phi_l(u_{l,s})$ ([Sequential Inference](#))
 - 6: $u_{l,s+1} \leftarrow u_{l,s} - \gamma_l e_{l,s} + \gamma_{l+1} \phi'_l(u_{l,s}) \circ W_{l+1}^\top e_{l+1,s}$
-

Additional Experiments with Figure 3 Figure S.13 presents the results of the same experiment shown in Figure 3 (Right), but with the CIFAR-10 dataset and the VGG5 model. It is evident that even with CIFAR-10 and VGG5, μP achieves higher accuracy compared to SP and NTK.

B.2 Target Propagation

B.2.1 Additional Experiments on $\mu\text{Transfer}$ for PC

Feedback Network As discussed in Section A.5, stable parametrization is crucial not only for feedforward but also for feedback networks. We verified this with μP , as shown in Figures S.14 and S.15 .

DRL [Meulemans et al. \[2020\]](#) proposes the difference reconstruction loss (DRL) for constructing feedback networks. In Figure S.16 , we empirically confirm that our μP works effectively with DRL when training an MLP on FashionMNIST.

Training samples As with PC, in the case of TP, Figure 7 uses 1024 training samples. Similar results were observed when using the full training dataset, as shown in Figure S.17 .

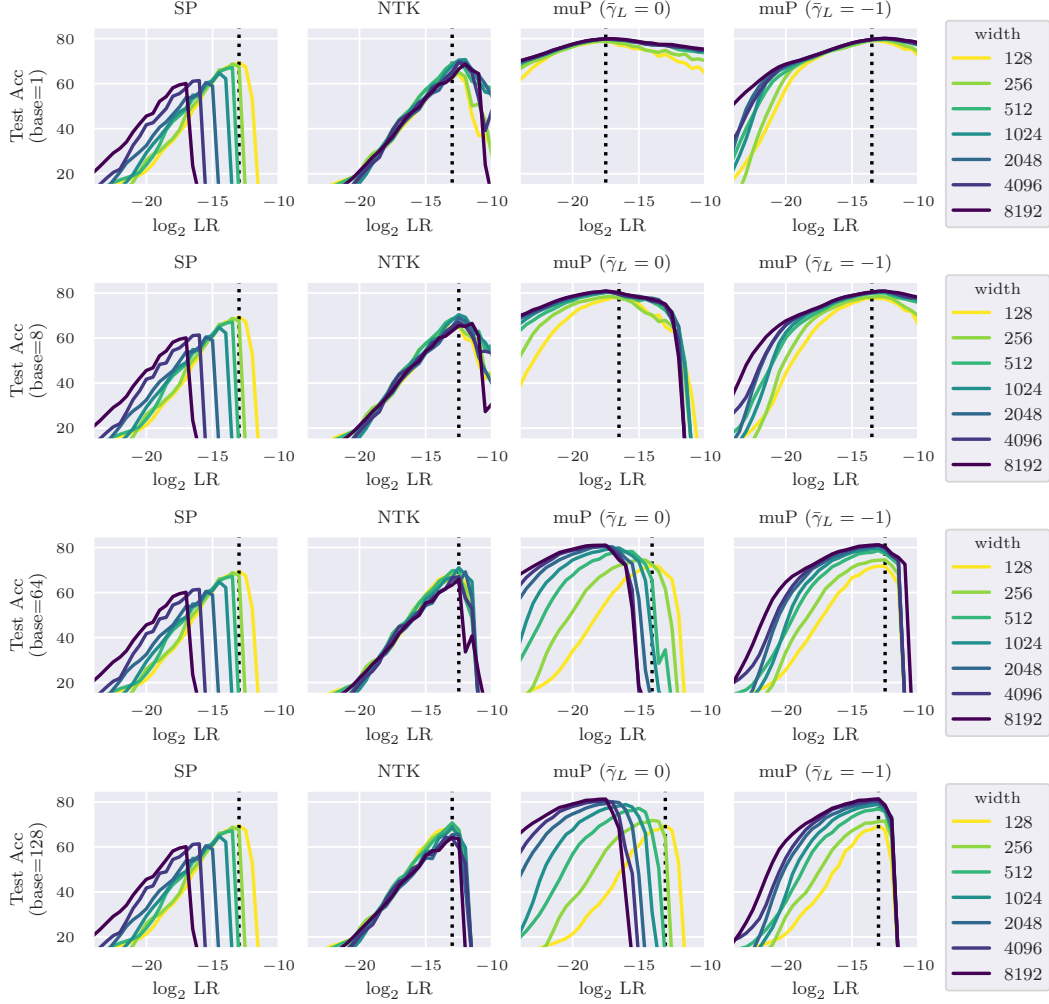


Figure S.10 : **When the base width M' is large, μP with $\bar{\gamma}_L = 0$ tends to fail with μ transfer.** We train 3-layer MLP on FashionMNIST. This suggests that μP with $\gamma_L = -1$ should be used when setting the base width, even with F-ini. The inference is performed for 100 iterations.

C Experimental Settings

Architecture and dataset We trained the following three models:

- **MLP:** We trained a 3-layer multilayer perceptron (MLP) with Tanh activation. The MLP models do not include bias.
- **CNN:** We trained 3-layer CNN with Tanh activation. The models consist of a two-layer convolutional layers and a linear layer. We trained with different hidden widths where the width is proportional to the input dimension of the output layer. (For example, when the width is set to 4, the input dimension of the final layer is 512.) Max pooling is applied after the activation function.
- **VGG5:** We trained a VGG-like model consisting of 4 convolutional blocks and 3 linear blocks, based on the structure described in [Pinchetti et al., 2024]. When the width is set to 8, it matches the VGG5 model in Pinchetti et al. [2024], with the channel sizes being [128, 256, 512, 512].

Dataset and batch size. We used FashionMNIST and CIFAR-10 datasets without applying any data augmentation. The settings for batch size and training samples were as follows:

- **PC** In the experiments on μ Transfer, FashionMNIST was generally trained with 1024 training samples and a batch size of 1024, except for Figure S.8 . However, when training VGG5, the

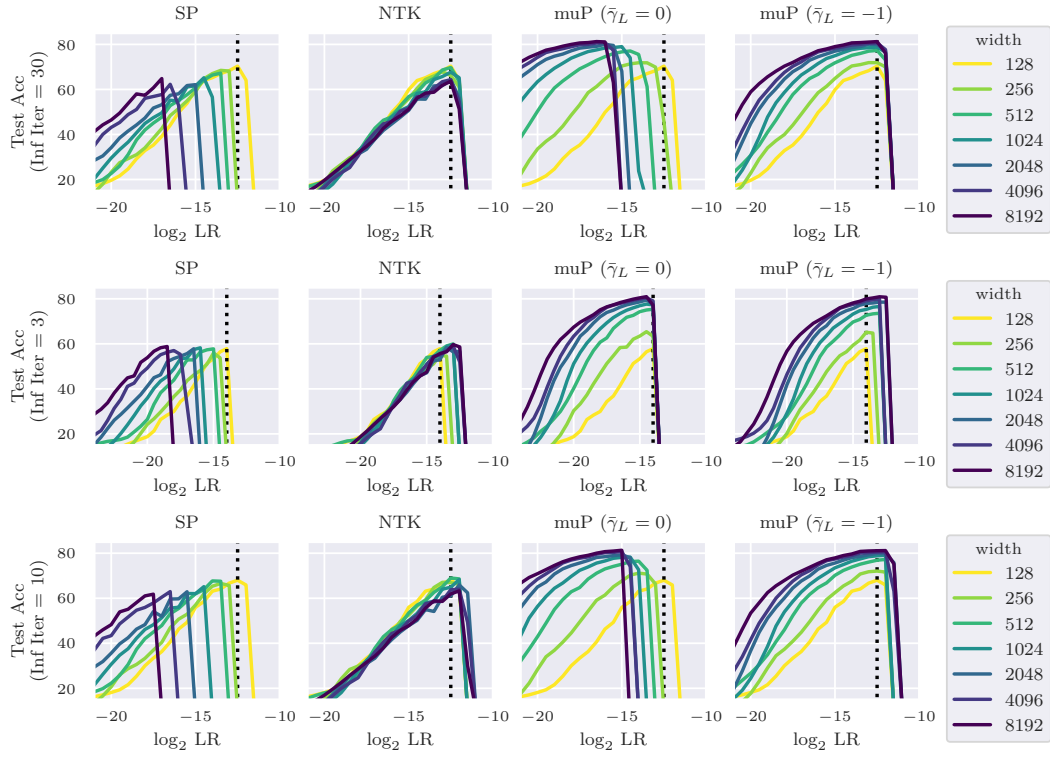


Figure S.11 : μP with $\bar{\gamma}_L = -1$ maintains high inference stability and successfully performs μ -transfer even with a large number of inference iterations. We conducted the experiment shown in Figure S.10 with varying numbers of inference iterations. Even with a larger number of inference iterations, μP with $\gamma_L = -1$ consistently transfers the learning rate across different widths.

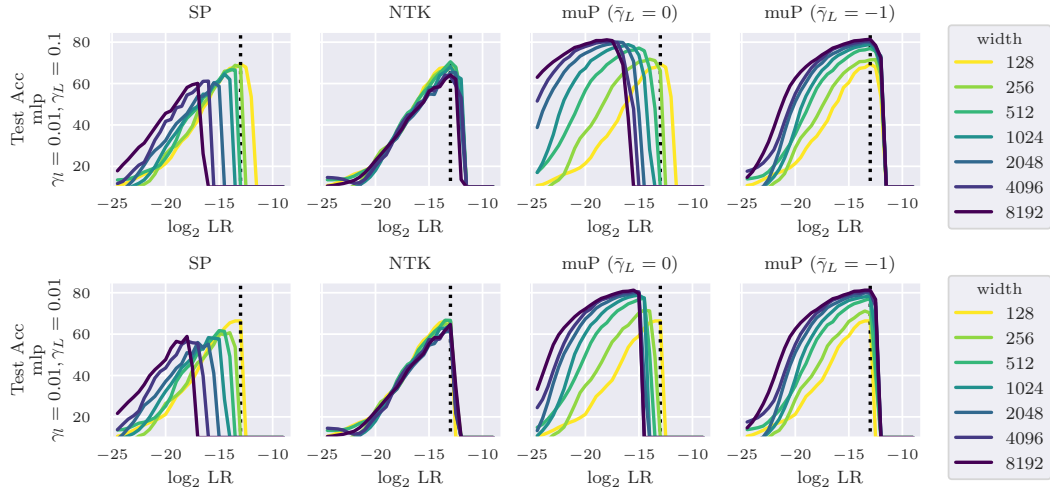


Figure S.12 : μP for PC also transfers learning rates across widths in synchronous inference. μP for PC can also be applied in synchronous inference. Note that when the base width is set to 1, as in SI, the learning rate does not transfer in μP with $\bar{\gamma}_L = 0$.

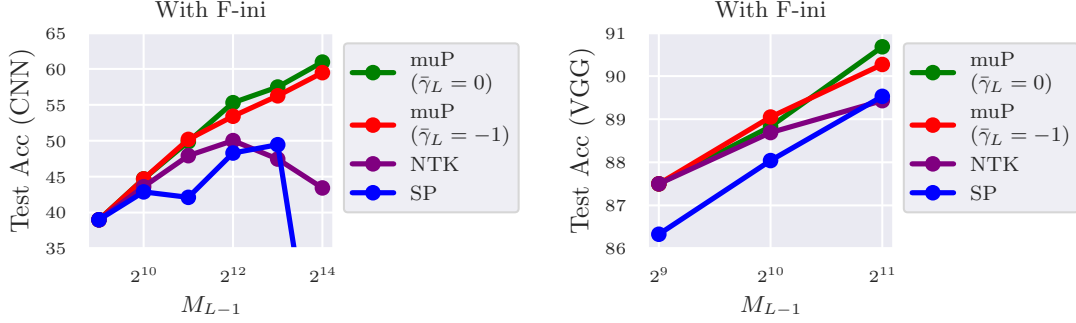


Figure S.13 : $\mu\mathbf{P}$ scales better than SP and NTK. We trained a CNN by PC with F-ini and a VGG5 on the full FashionMNIST dataset. The "wider is better" principle holds for $\mu\mathbf{P}$.

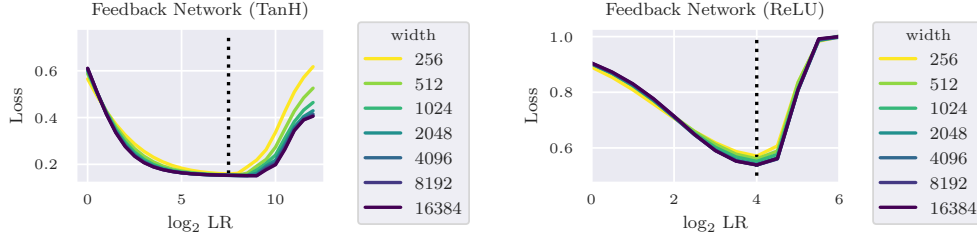


Figure S.14 : **Learning rate transfer in Feedback networks.** We demonstrate that the learning rate in feedback networks transfers effectively across widths using toy data. Both the feedforward and feedback networks include a Tanh/ReLU activation function following the linear layer.

batch size was reduced to 64 due to memory constraints. In the experiment verifying the scaling of $\mu\mathbf{P}$ with respect to width (Figure 3), all training samples were used, with a batch size of 1024.

- **TP** In Figures 6 and 7, we trained 3-layer MLP using 1024 training samples. Note that in Figure S.17 in the Appendix, FashionMNIST and CIFAR-10 were trained using the full datasets.

Training recipe Weight decay was not applied during the parameter updates for feedforward networks. For SGD, the momentum was set to 0.9, and for AdamW, the parameters (β_1, β_2) were set to (0.9, 0.99).

- **PC** The reduction mode for the loss function was set to "sum" to align the order of all terms in the free energy function.
- **TP** For feedback networks, weight decay was set to 10^{-4} and the learning rate for the target was set to $\hat{\eta} = 0.01$. Before starting the main training, only the feedback network was trained for 5 epochs with the feedforward network fixed.

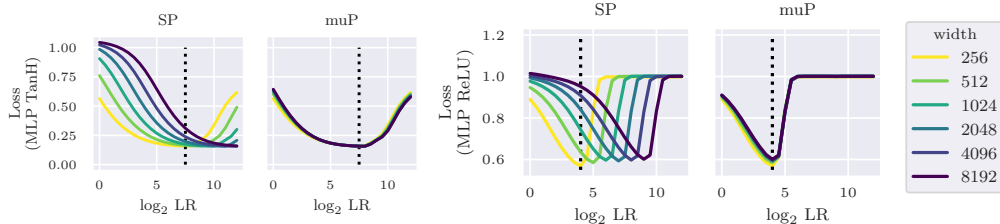


Figure S.15 : **Learning rate transfer in Feedback networks (output layer).** We show that the learning rate in feedback networks transfers across widths using toy data. Unlike the hidden layers, the learning rate in the output layer does not transfer under the default setting, which requires $\mu\mathbf{P}$ scaling. Both the feedforward and feedback networks include a Tanh/ReLU activation function after the linear layer.

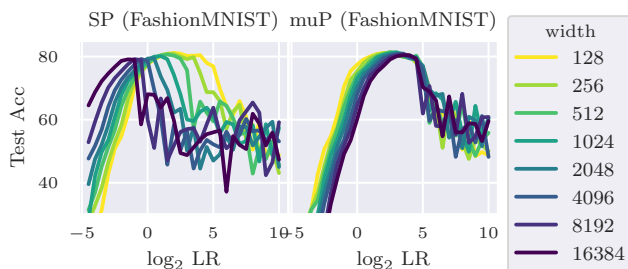


Figure S.16 : **Even when training the feedback network with DRL, $\mu\mathbf{P}$ demonstrates greater stability compared to SP.** We trained a 3-layer MLP on the FashionMNIST using DRL. While SP exhibits a shift in the maximum learning rate as the model width increases, $\mu\mathbf{P}$ consistently transfers the optimal learning rates across different widths.

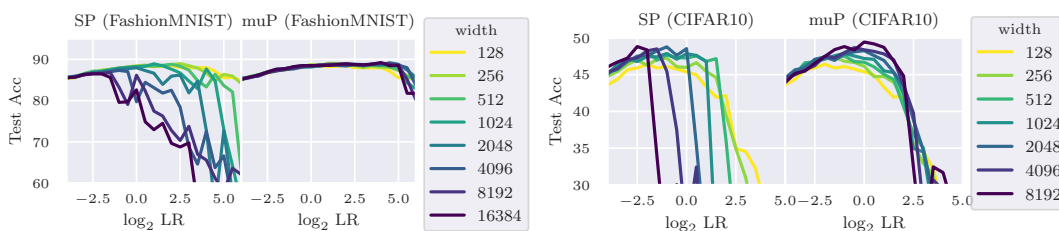


Figure S.17 : **$\mu\mathbf{P}$ for TP remains stable regardless of the dataset or the number of training samples.** We trained a 3-layer MLP on both FashionMNIST and CIFAR-10 using the full training samples. With $\mu\mathbf{P}$, the learning rate successfully transfers across widths, ensuring that the maximum learning rate remains consistent regardless of the model width.